Science
AAAS

Supplementary Materials for

A tool kit of highly selective and sensitive genetically encoded neuropeptide sensors

Huan Wang *et al*.

Corresponding author: Yulong Li, yulongli@pku.edu.cn

Science **382**, eabq8173 (2023)
DOI: 10.1126/science.abq8173

The PDF file includes:

Figs. S1 to S17
Tables S1 to S4
References

Other Supplementary Material for this manuscript includes the following:

MDAR Reproducibility Checklist
Movie S1
Data S1 and S2

Fig. S1. Membrane trafficking of peptide GPCRs with ICL3 grafted from different sensors.

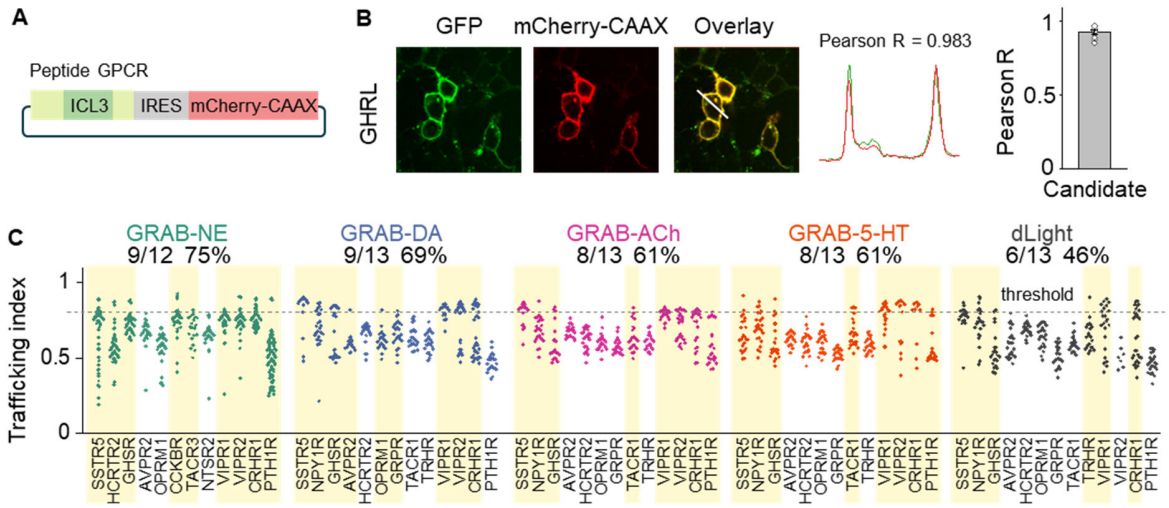

Fig. S1. Membrane trafficking of peptide GPCRs with ICL3 grafted from different sensors.

(**A**) Schematics of the construct for membrane trafficking screening.

(**B**) Example fluorescence images and intensity line scan profiles of a chimeric GPCR (ghrelin receptor, GHSR) grafted with dLight ICL3 (green), mCherry-CAAX (red), and merged image in the presence of ghrelin (1 μM). The white line indicated the ROI for intensity profiling, and Pearson R was calculated. The averaged Pearson R was used to indicate the membrane trafficking index of sensor variants.

(**C**) Summary of the membrane trafficking index measured for peptide GPCR chimeras containing the ICL3 transplanted from the indicated sensors. The number and percentage of GPCR chimeras with a maximum trafficking index >0.8 (dashed horizontal line) are shown. Each data point represents the average of 100-300 cells measured in one well.

Fig. S2. Development and optimizations of GRAB sensors for detecting neuropeptides.

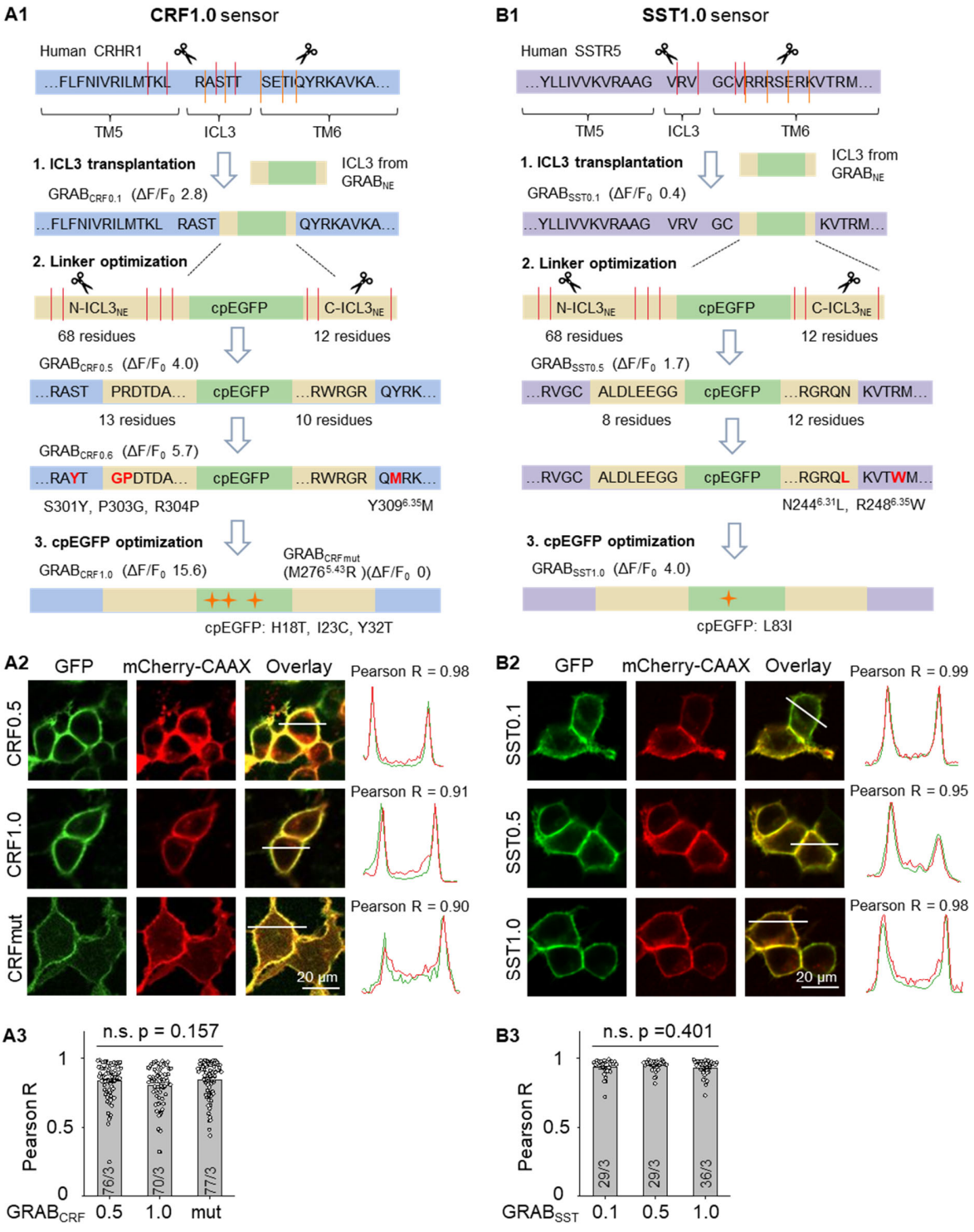

Fig. S2. Development and optimization of GRAB sensors for detecting neuropeptides.

(**A-B**) Flow charts showing the 3-step development process (**A1** and **B1**), representative images (**A2** and **B2**) and group summary (**A3** and **B3**) of the membrane trafficking properties for selected sensor candidates during optimization for CRF1.0 (**A1-A3**) and SST1.0 (**B1-B3**). Responses to the saturated concentration of peptide ligands of candidate sensors were shown alongside each step. One-way ANOVA test, $F(2, 220) = 1.865$, $P=0.1573$ between CRF0.5, CRF1.0 and CRFmut (A3); $F(2, 91) = 0.9230$, $P=0.4010$ between SST0.1, SST0.5 and SST1.0 (B3).
Scale bars, 20 μm.

Fig. S3. Full amino acid sequences of all six GRAB peptide sensors.

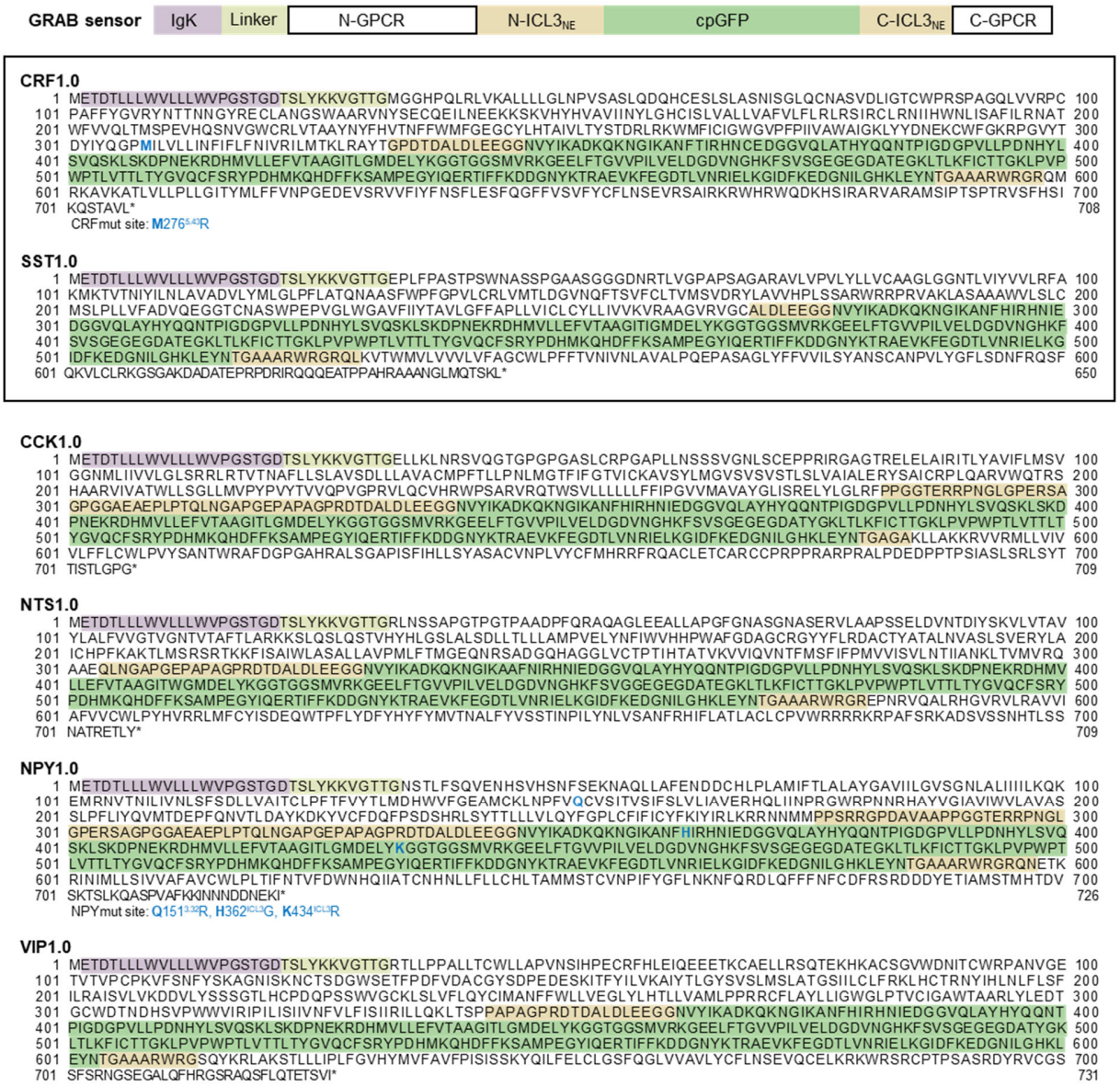

Fig. S3. Full amino acid sequences of all six GRAB peptide sensors.

The sequence shaded in green indicates cpGFP, and the sequences shaded in yellow indicate the ICL3 linkers derived from the GRAB-NE sensor. The M→R mutation in CRF1.0 used to generate CRFmut is shown in blue. Also shown are the IgK and linker sequences. Note that the numbering used in the figure corresponds to the start of the IgK leader sequence.

Fig. S4. Characterization of SST1.0 and CRF1.0 expressed in HEK293T cells.

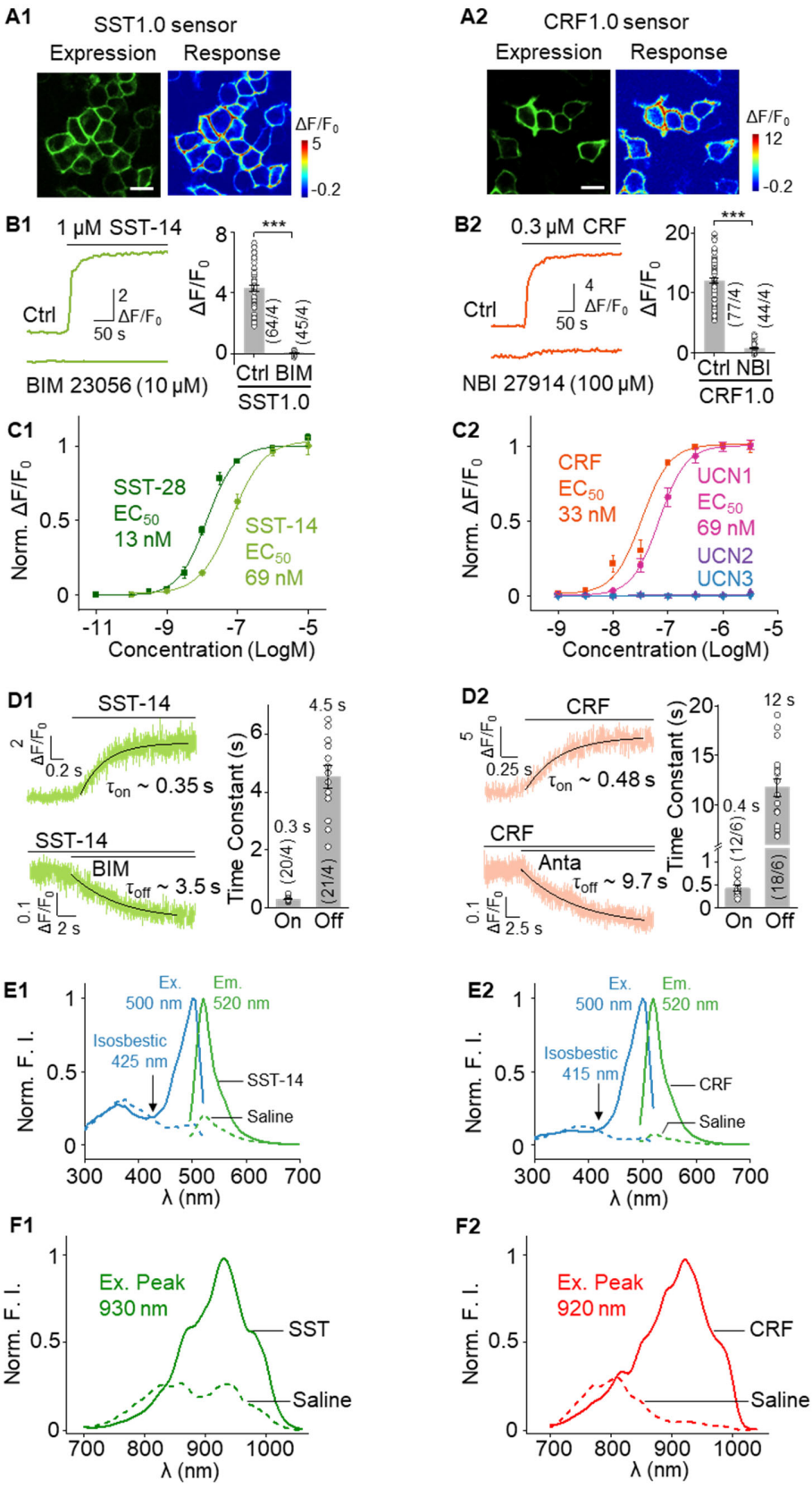

Fig. S4. Characterization of SST1.0 and CRF1.0 expressed in HEK293T cells.

(**A**) Representative images of HEK293T cells expressing SST1.0 (**A1**) or CRF1.0 (**A2**), and the response to the application of SST-14 (1 μM) and CRF (300 nM), respectively. Scale bars, 20 μm.
(**B**) Example fluorescence traces (left) and summary data (right) of HEK293T cells expressing SST1.0 (**B1**) or CRF1.0 (**B2**); where indicated, the cells were pre-incubated with saline (Ctrl) or the antagonist BIM 23056 (10 μM) or NBI 27914 (100 μM); n = 44-125 cells from 3-4 coverslips.
(**C**) Normalized dose-response curves of HEK293T cells expressing SST1.0 (**C1**) or CRF1.0 (**C2**) in response to the respective ligand (n = 3 wells containing 100-300 cells per well).
(**D**) Representative traces (left) and summary of τ_{on} and τ_{off} (right) of the SST1.0 (**D1**) and CRF1.0 (**D2**) response. The indicated ligands and antagonists were locally puffed onto sensor-expressing cells, and high-speed line scanning was used to measure the fluorescence response. Where indicated, SST-14 (1 mM) and CRF (100 μM) for measuring signal increase; BIM 23056 (100 μM), Antalarmin (100 μM), SST-14 (1 μM) and CRF (100 nM) were applied (n = 12-21 cells from 4-6 cultures)
(**E**) Excitation (Ex) and emission (Em) spectra of SST1.0 (**E1**) and CRF1.0 (**E2**) expressed in HEK293T cells, measured in the presence (solid curves) and absence (dashed curves) of SST-14 (10 μM) and CRF (1 μM), respectively.
(**F**) Two-photon excitation cross-sections of the SST1.0 (**F1**) and CRF1.0 (**F2**) sensors expressed in HEK293T cells in the presence of saline (dashed lines) or the corresponding ligand (solid lines). Normalized fluorescence intensity is plotted on the *y-axis*.

Fig. S5. Expression and localization of SST1.0 sensor in cultured neurons.

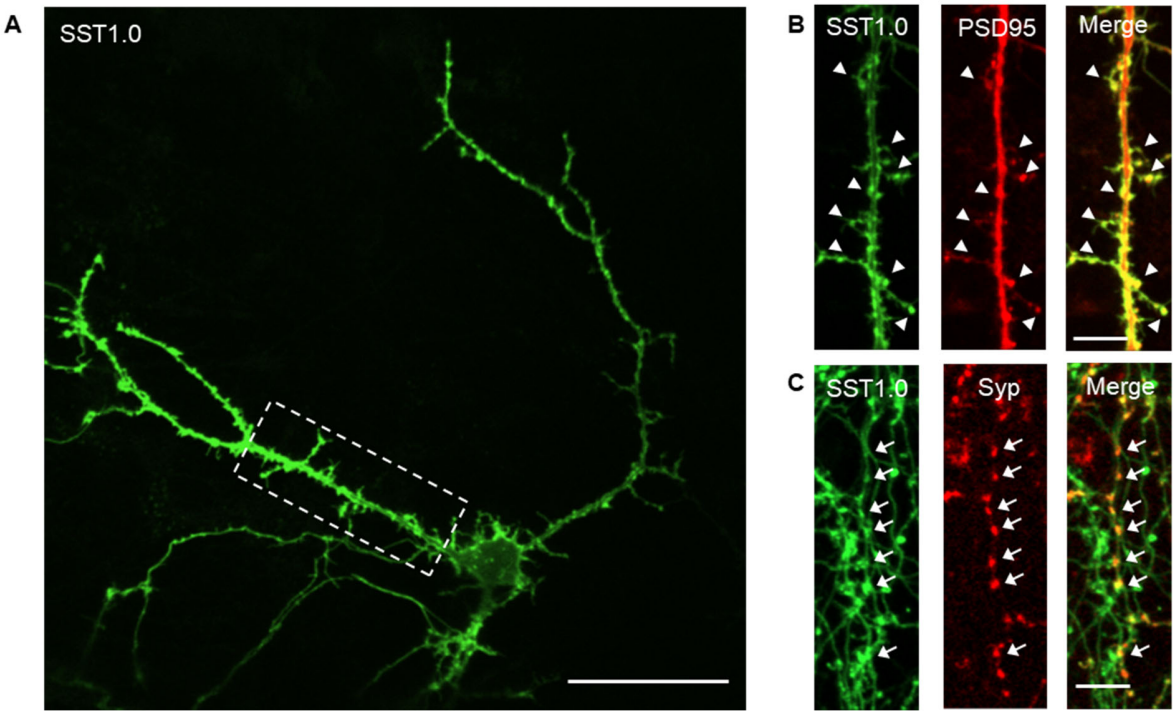

Fig. S5. Expression and localization of the SST sensor in cultured neurons.

(**A**) Representative fluorescence microscopy images of primary cultured rat cortical neurons expressing SST1.0. White dashed rectangle regions were zoomed-in in the up panels of (**B**). Scale bars, 50 μm.

(**B** and **C**) Fluorescence images of neurons expressing SST1.0 (green) and either PSD95–mScarlet (top row, red) or synaptophysin (Syp)–mScarlet (bottom row, red). In the top row, arrowheads indicate dendrites and dendritic spines; in the bottom row, arrows indicate axons; Similar results were observed for more than 10 neurons from 3 transfections. Scale bars, 10 μm.

Fig. S6. Downstream signal of cells expressing peptide sensors.

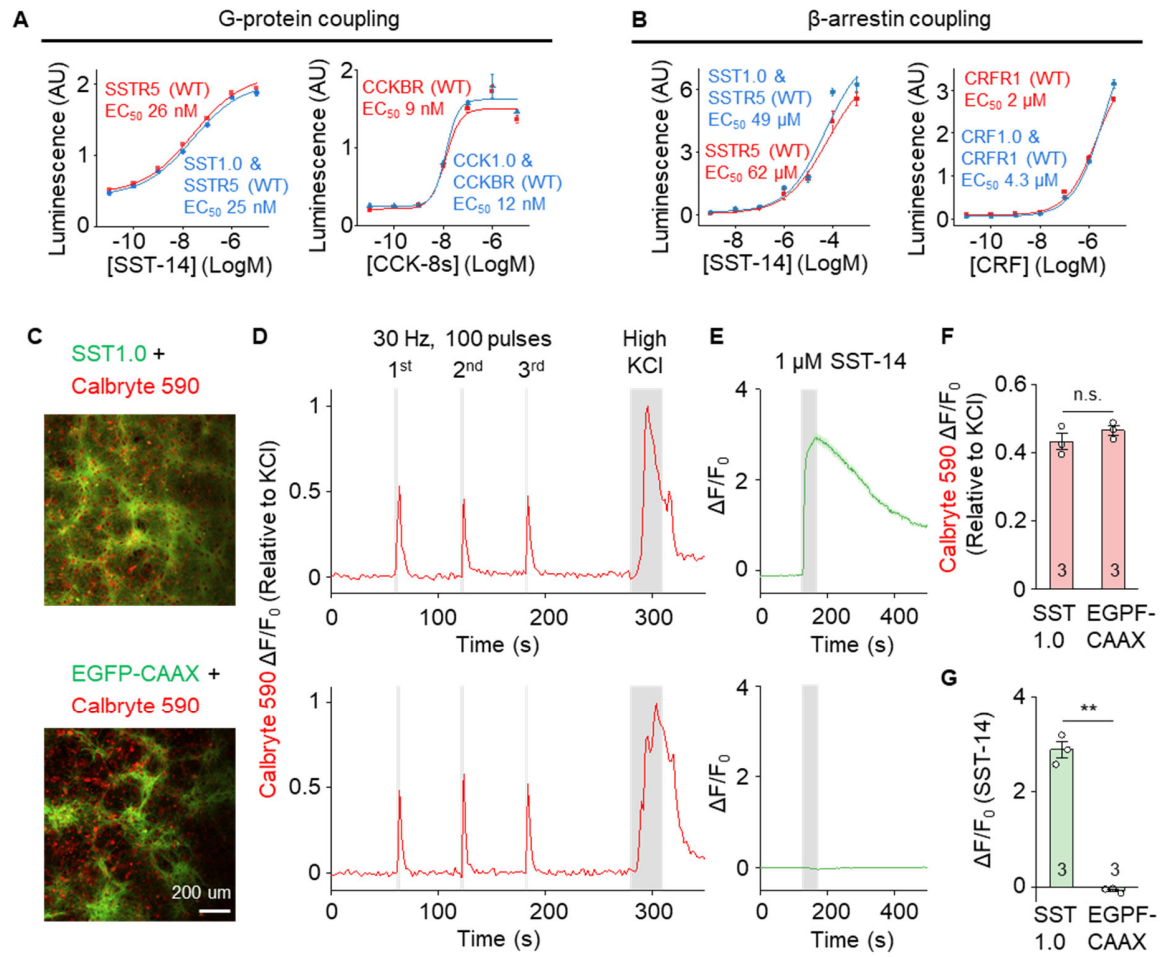

Fig. S6. Downstream signal of cells expressing peptide sensors.

(**A** and **B**) G protein and β-arrestin coupling were measured using the split-luciferase complementation assay (**A**) or the Tango assay (**B**) in cells expressing either the wild-type peptide receptor (red), or wild-type peptide receptor with peptide sensor (blue) in the presence of the indicated concentrations of the ligand; n = 3 wells each. The data of wilt-type groups were replotted from the Figure 2F and 2G.

(**C-E**) Representative fluorescence images of cultured rat cortical neurons expressing SST1.0 (top) or EGFP-CAAX (bottom) and loaded with dye Calbryte 590 (red) (**C**), traces of Calbryte 590 $\Delta F/F_0$ in response to repeated field stimulation or high KCl perfusion (**D**), and traces of SST1.0 (top) or EGFP-CAAX (bottom) $\Delta F/F_0$ in response to 1 μM SST-14 (**E**). Scale bars, 200 μm.

(**F** and **G**) Group summary of calcium response (**F**) and $\Delta F/F_0$ of green channels to 1 μM SST-14 (**G**). (n = 3 neuron cultures) Student's t-test performed, p = 0.3209 (**F**), p = 0.0028 (**G**).

Fig. S7. Expression of peptide sensors does not alter transcriptomes.

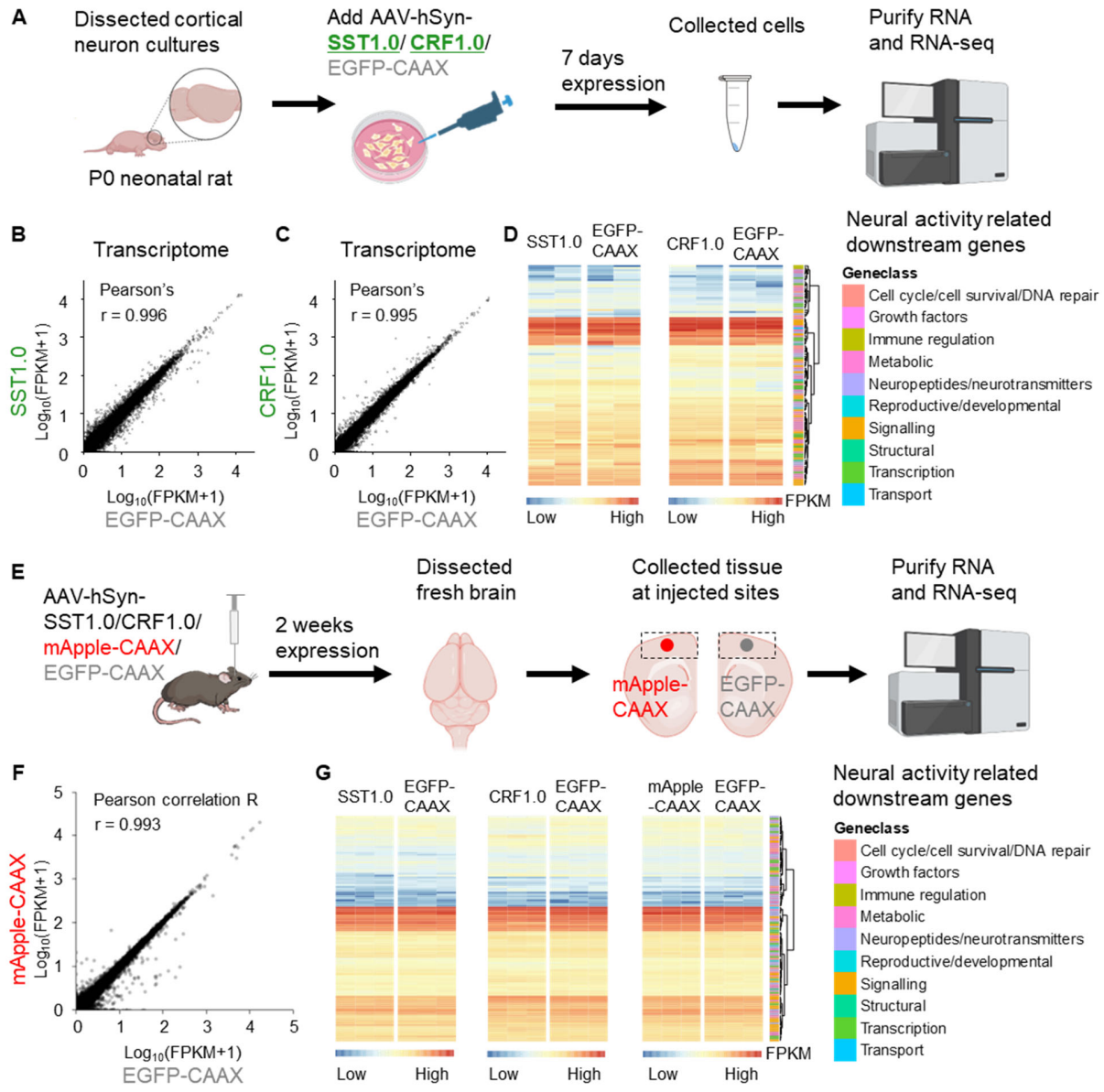

Fig. S7. Expression of peptide sensors does not alter transcriptomes.

(**A**) Schematic of cultured rat cortical neurons expressing SST1.0, CRF1.0 or EGFP-CAAX for 7 days, then the cells were collected to extract RNA for sequencing.

(**B** and **C**) RNA-seq analysis shows that GRAB peptide sensor did not alter the general transcriptome of cultured neurons. Comparisons of transcriptomes between neurons expressing SST1.0 or EGFP-CAAX (**B**) and between CRF1.0 or EGFP-CAAX (**C**).

(**D**) Comparison of selected neural activity-related CREB responsive gene expression levels between neurons expressing GRAB sensors or EGFP-CAAX control.

(**E**) Schematic of mice brain expressing SST1.0, CRF1.0, mApple-CAAX or EGFP-CAAX for 2 weeks, then motor cortex tissue was collected for RNA sequencing.

(**F**) Comparisons of transcriptomes between motor cortex expressing mApple-CAAX or EGFP-CAAX.
(**G**) Comparison of selected neural activity related CREB responsive genes expression levels between motor cortex expressing GRAB sensors, mApple-CAAX or EGFP-CAAX control.
Pearson′s correlation coefficient analysis was used to evaluate the differential RNA expression (**B**, **C** and **F**).

Fig. S8. Expression of peptide sensors does not alter native GPCR.

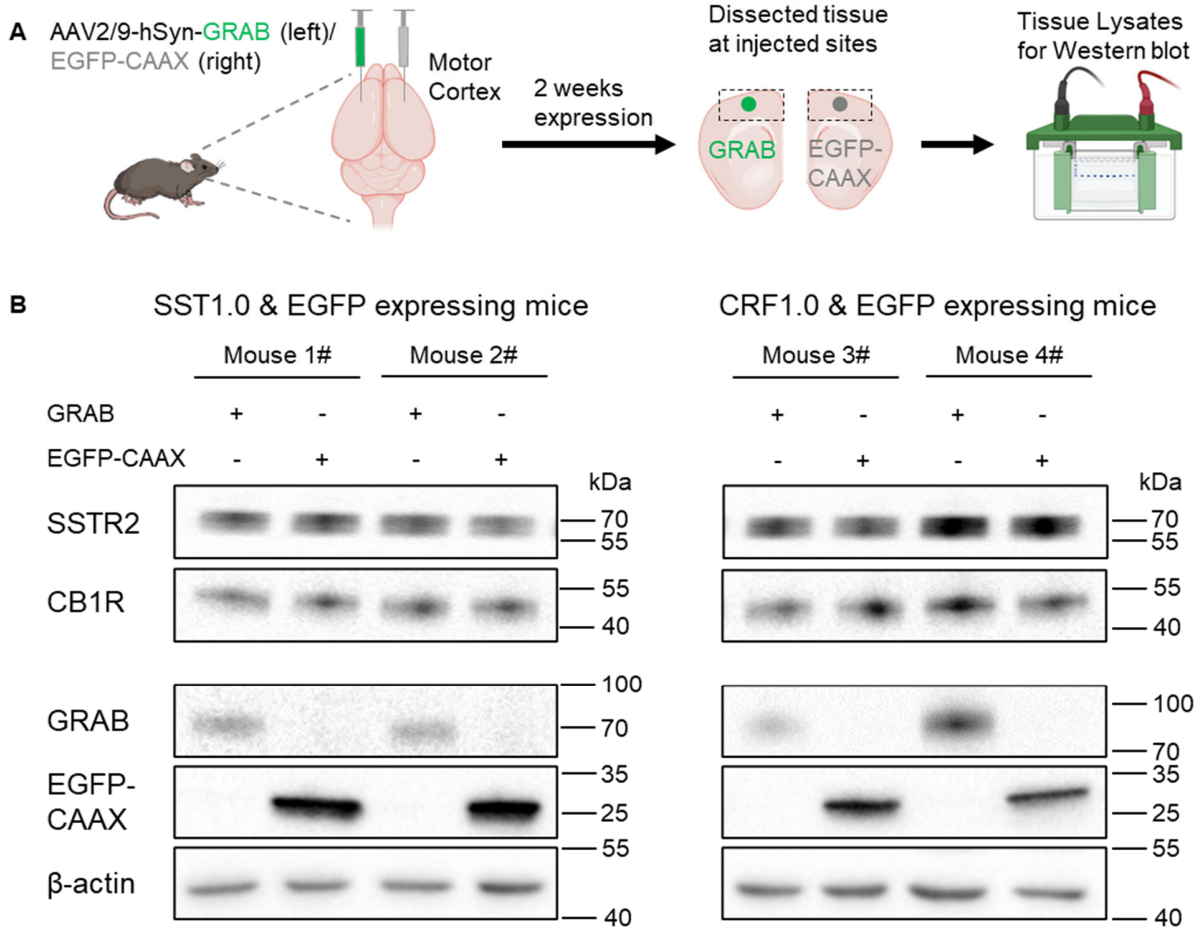

Fig. S8. Expression of peptide sensors does not alter the native GPCR expression.

(**A**) Schematic of mice motor cortex expressing GRAB sensors (left) or EGFP-CAAX (right) for 2 weeks, the tissue was collected for Western blot.

(**B**) Western blot shows that expressing GRAB peptide sensor did not alter the protein level of native SSTR2 and CB1R GPCRs.

Fig. S9. Expression of peptide sensors does not alter the native SSTR2 GPCR distribution.

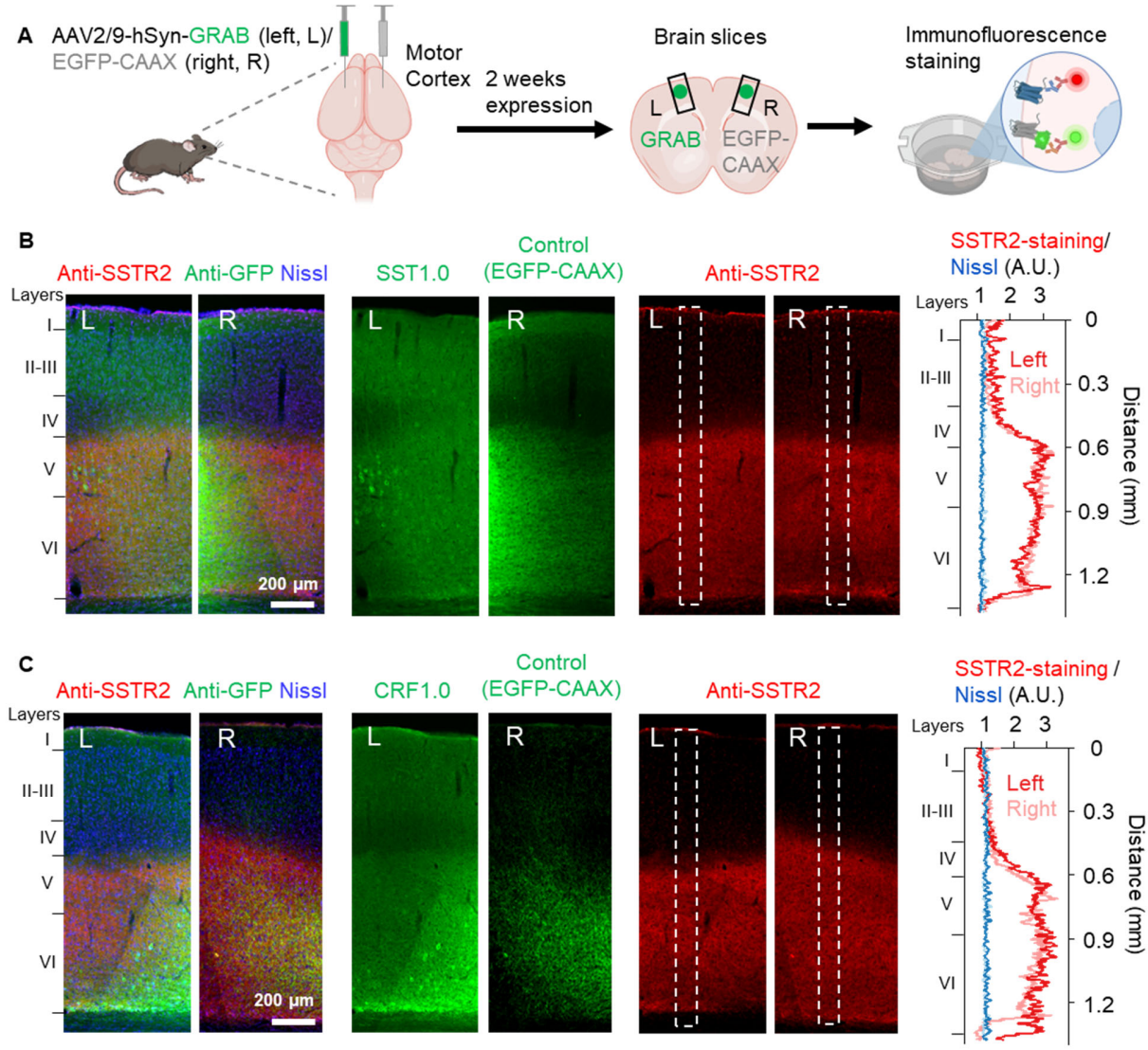

Fig. S9. Expression of peptide sensors does not alter the native SSTR2 GPCR localization.

(**A**) Schematic diagram depicting the experiment design.

(**B and C**) Representative fluorescence images showing the merged signal (left), immunoactivities of GFP (middle, green) and SSTR2 (right, red) of mice motor cortex expressing GRAB sensors (SST1.0(**B**) and CRF1.0 (**C**)) at left motor cortex (L) and EGFP-CAAX at right motor cortex (R). The approximate layers of neocortex are indicated. Intensity profiles of white dashed rectangle regions of SSTR2 immunoactivities (red) and Nissl staining (blue) from dura to the deep cortex were plotted. Scale bars, 200 μm.

Fig. S10. Validation of the SST1.0 sensor in culture neurons and pancreatic islets.

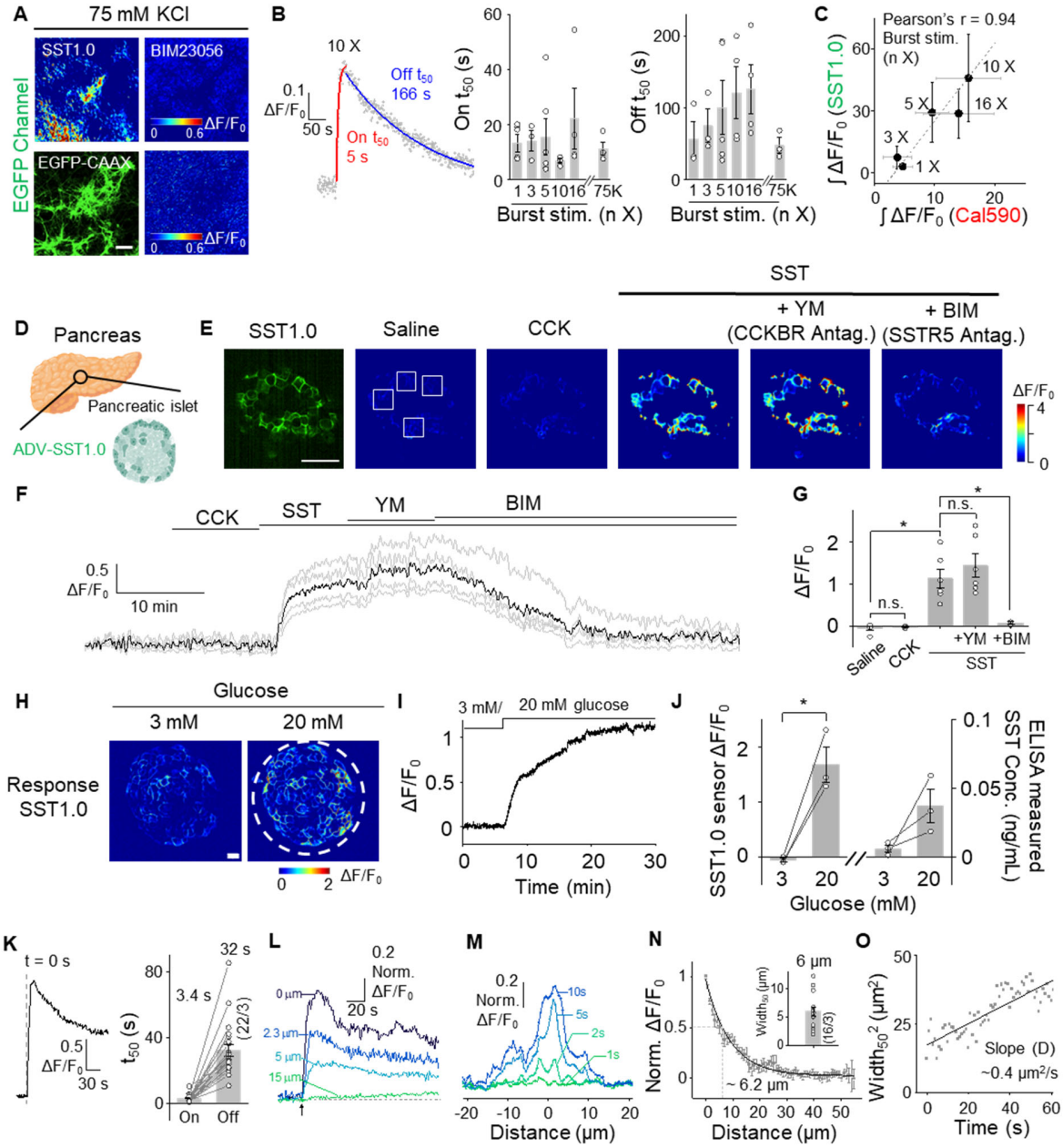

Fig. S10. Validation of the SST1.0 sensor in culture neurons and pancreatic islets.

(**A**) Representative fluorescence images of rat cortical neurons expressing SST1.0 (top row) or EGFP-CAAX (bottom row); 75 mM K^+ was applied by perfusion in the absence (left column) or presence (right column) of the SST receptor antagonist BIM (5 μM). Scale bars, 100 μm.

(**B**) Representative time course (left) and summary of the rise and decay half-times (t_{50}) of the fluorescence change (right) measured in SST1.0-expressing neurons in response to burst stimuli and 75 mM K^+; n = 3-5 cultures containing 20-40 ROIs per culture.

(**C**) Change in SST1.0 fluorescence plotted against the Calbryte-590 signal measured in response to the indicated number of burst stimuli.
(**D**) Schematic diagram depicting the experimental strategy in which pancreatic islets were isolated, and infected with adenoviruses expressing SST1.0.
(**E**) Expression and pseudocolor responses measured in a mouse pancreatic islet expressing SST1.0 in control solution (saline supplemented with 250 μM diazoxide), 1 μM CCK-8s, and 1 μM SST-14 in the absence and presence of the CCKBR antagonist YM022 (10 μM) or the SSTR5 antagonist BIM23056 (10 μM). White squares indicate the ROIs for quantification. Scale bar, 50 μm.
(**F**) Average (black trace) and raw (gray traces) fluorescence responses measured at the 4 ROIs shown in (**E**).
(**G**) Summary of the change in SST1.0 fluorescence measured in SST1.0-expressing islets under the indicated conditions; n = 3-6 islets each.
(**H**) Pseudocolor images of a mouse islet expressing SST1.0 in the presence of 3 mM and 20 mM glucose. The dashed circle indicates the islet. Scale bar, 20 μm.
(**I**) Representative fluorescence trace of SST1.0-expressing mouse islets in the presence of 3 mM and 20 mM glucose.
(**J**) Summary data of mouse islets SST release measured by SST1.0 sensor or SST concentration in culture medium measured by ELISA in the presence of 3 mM and 20 mM glucose. Student's t-test performed, p=0.0259 for SST1.0 group; p=0.1523 for ELISA group.
(**K**). Left: example fluorescence response trace corresponding to the single burst. Right: summary of the rise and decay t_{50} values measured for 22 burst events in 3 islets.
(**L** and **M**) Representative temporal dynamics (**L**), and spatial dynamics (**M**) of the SST1.0 fluorescence response measured during a single burst. The arrow in (**L**) indicates time 0. The traces in (**L**) and (**M**) correspond to the indicated distances and times, respectively.
(**N**) Normalized fluorescence responses measured at 10 s fitted with a single-exponential function, showing a signal $width_{50}$ of approximately 6.2 μm. The inset shows the summary $width_{50}$ data (n = 16 burst events from 3 islets).
(**O**) Distribution of the $(width_{50})^2$ over time, fitted to a linear function with a slope of 0.4 $\mu m^2/s$.

Fig. S11. The CRF1.0 specifically detects the CRF peptide in brain slices.

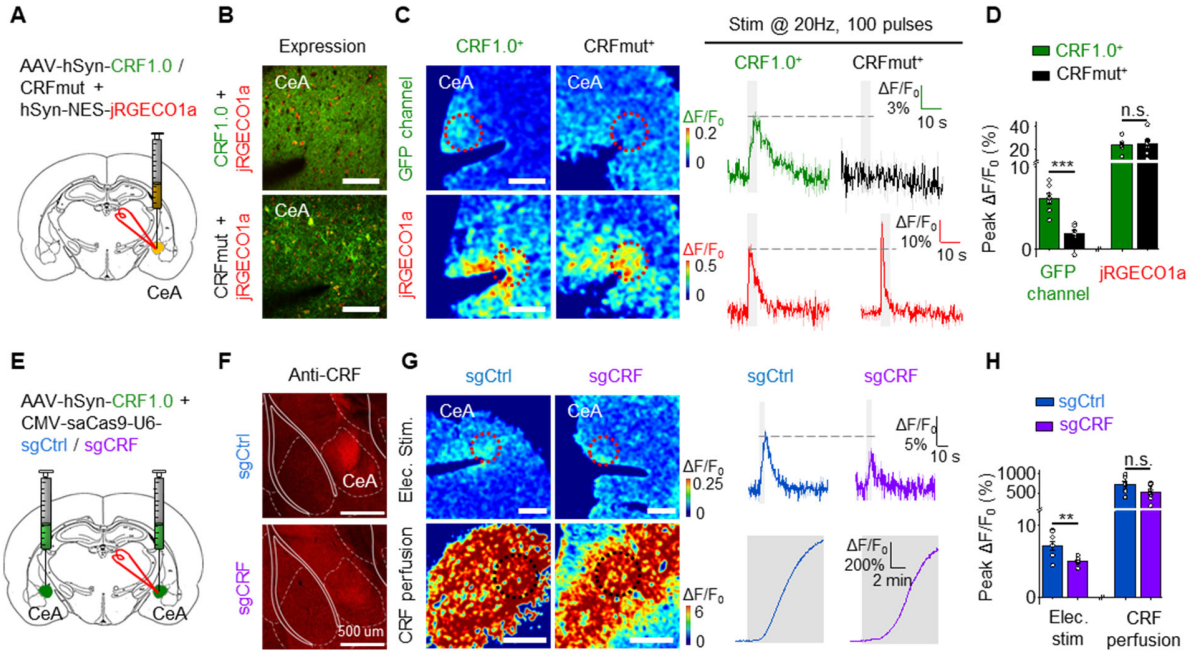

Fig. S11. The CRF1.0 specifically detects the CRF peptide in brain slices.

(**A-D**) Schematic diagram (**A**), example 2-photon expression images (**B**), representative pseudocolor images and traces (**C**), and summary of peak responses (**D**) of acute brain slices expressing jRGECO1a with CRF1.0 or CRFmut at CeA, treated with electric stimulation at 20 Hz. n=7 slices from 3 mice ($CRF1.0^{+}$) and n=7 slices from 3 mice ($CRFmut^{+}$). Student's t-test performed; p = 0.0002 (GFP channel) and p = 0.94 (jRGECO1a), ***p<0.001. Scale bars, 100 μm.

(**E**) Schematic illustration of experiment design. AAVs expressing CRF1.0 and saCas9-gRNA were injected into CeA bilaterally. Electric stimuli were used to activate the CeA neurons of acute brain slices.

(**F**) Representative images of CRF immunoreactivity of the sgCtrl (control) and sgCRF (KO) groups. Scale bars, 500 μm.

(**G**) Representative pseudocolor response images and traces of CRF1.0 in response to electric stimuli and CRF perfusion (1 μM) of the sgCtrl (control) and sgCRF(KO) groups. Scale bars, 100 μm.

(**H**) Group summary of peak $\Delta F/F_0$ for CRF1.0 sensor of the sgCtrl and sgCRF groups. n=8 slices from 3 mice (sgCtrl) and n=8 slices from 3 mice (sgCRF). Student's t-test performed; p=0.009 (Elec. Stim) and p = 0.07 (CRF perfusion), **p<0.01.

Summary data are presented as the mean ± SEM.

Fig. S12. Expression of the peptide sensor does not disturb neuronal activities in brain slices.

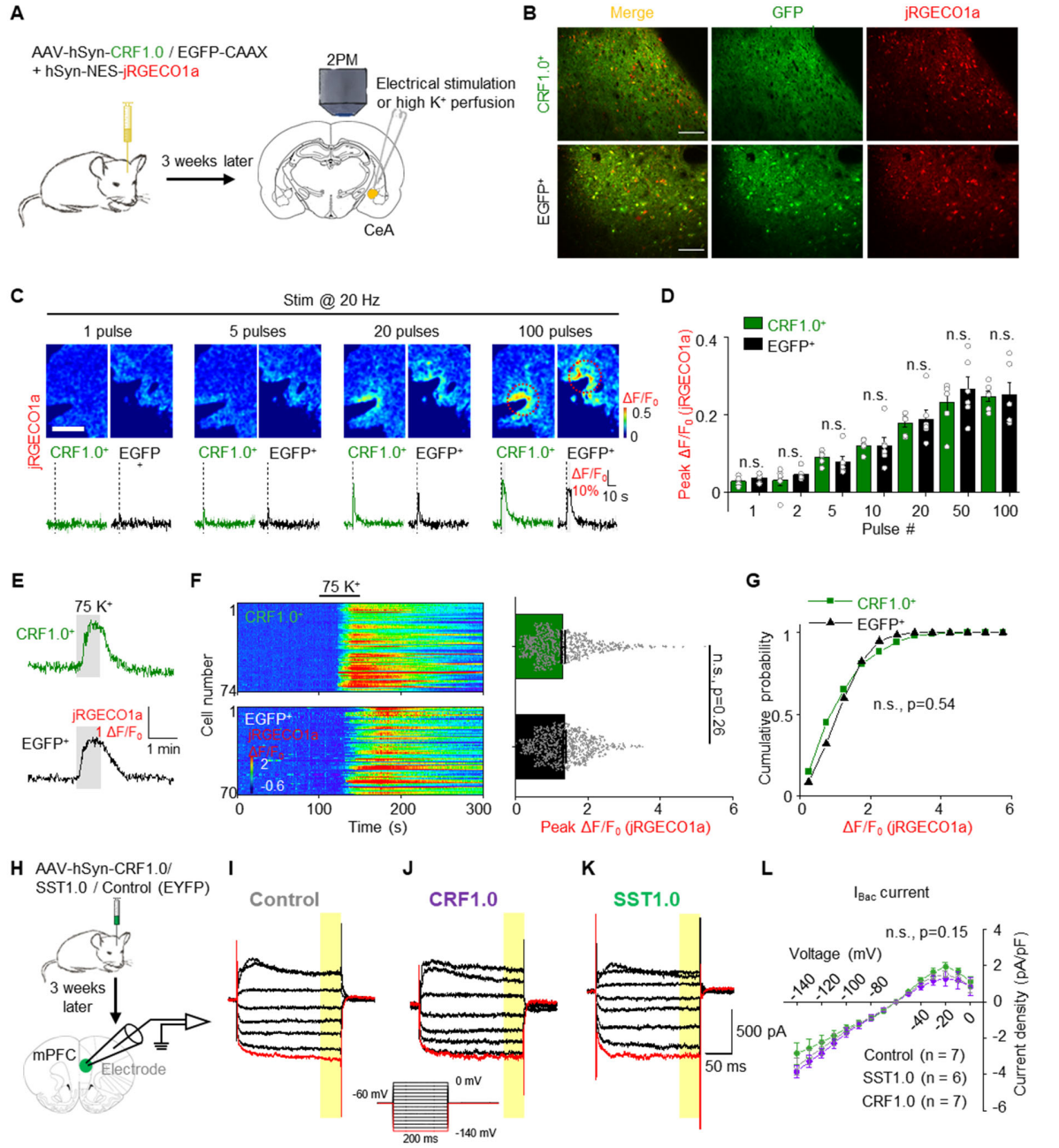

Fig. S12. Expression of the peptide sensor does not disturb neuronal activities in brain slices.

(**A**) Schematic diagram of acute brain slices expressing jRGECO1a with CRF1.0 or EGFP-CAAX at CeA, treated with electric stimulation and high K^+ perfusion.

(**B**) Representative 2-photon fluorescence images of acute brain slices, showing expression of CRF1.0, EGFP-CAAX and jRGECO1a. Scale bars, 100 μm.

(**C**) Example pseudocolor images (top) and traces (bottom) of the change in jRGECO1a fluorescence in response to electric stimuli delivered at 20 Hz in ACSF. Scale bars, 100 μm.
(**D**) Summary of the peak responses of jRGECO1a signal in response to electric stimuli delivered at 20 Hz. CRF1.0^{+}: n=6 slices of 3 mice, EGFP^{+}: n=6 slices of 3 mice; Student's t-test, p=0.22, 0.34, 0.45, 0.99, 0.73, 0.43, 0.90 for 1, 2, 5, 10, 20, 50, 100 pulses group, respectively.
(**E**) Example traces showing the high K^{+} perfusion evoked calcium signals in neurons co-expressing CRF1.0 (green) or EGFP-CAAX (black).
(**F**) Left: pseudocolor change in jRGECO1a fluorescence in neurons co-expressing CRF1.0 (upper) or EGFP-CAAX (bottom) before and after the high K^{+} perfusion. Shown are 74 and 70 neurons in one slice each. Right: Summary of peak jRGECO1a $\Delta F/F_0$ measured in neurons co-expressing CRF1.0 (upper) or EGFP-CAAX (bottom). CRF1.0^{+}: n=515 cells from 8 slices of 3 mice; EGFP^{+}: n=672 cells from 9 slices of 3 mice. Student's t-test, p=0.26.
(**G**) Cumulative probability plot of jRGECO1a $\Delta F/F_0$ measured in neurons co-expressing CRF1.0 or EGFP-CAAX. Kolmogorov-Smirnov test, p=0.54.
(**H**) Schematic diagram depicting the experiment design of electrophysiology recording of layer 5 pyramidal neurons expressing SST1.0, CRF1.0 or EYFP in mice mPFC.
(**I-K**) Example traces of voltage-activated baclofen-induced potassium currents (I_{Bac}) measured in control (EYFP) neurons (**I**), CRF1.0-expressing neurons (**J**), and SST1.0-expressing neurons (**K**) during voltage steps (200 ms) from a holding potential of −60 mV to various test potentials (-140 to 0 mV, see inset). The $GABA_BR$ agonist baclofen-induced currents (I_{Bac}) were calculated by subtracting the constitutive currents under pre-treatment conditions from those recorded during baclofen perfusion. The highlighted region was utilized for calculating the amplitude of I_{Bac}.
(**L**) I/V relationship for the baclofen-induced currents (I_{Bac}) displayed inward rectification and similar reversal potential for neurons expressing SST1.0, CRF1.0 or EYFP (control) as indicated. n=7 neurons from 4 mice (Control); n=6 neurons from 4 mice (SST1.0); n=7 neurons from 3 mice (CRF1.0). Two-way ANOVA test, F (2, 17) = 2.147, p=0.15 between control, SST1.0 and CRF1.0 groups.
Summary data are presented as the mean ± SEM. n.s., not significant.

Fig. S13. CRF1.0 can detect endogenous CRF release using fiber photometry.

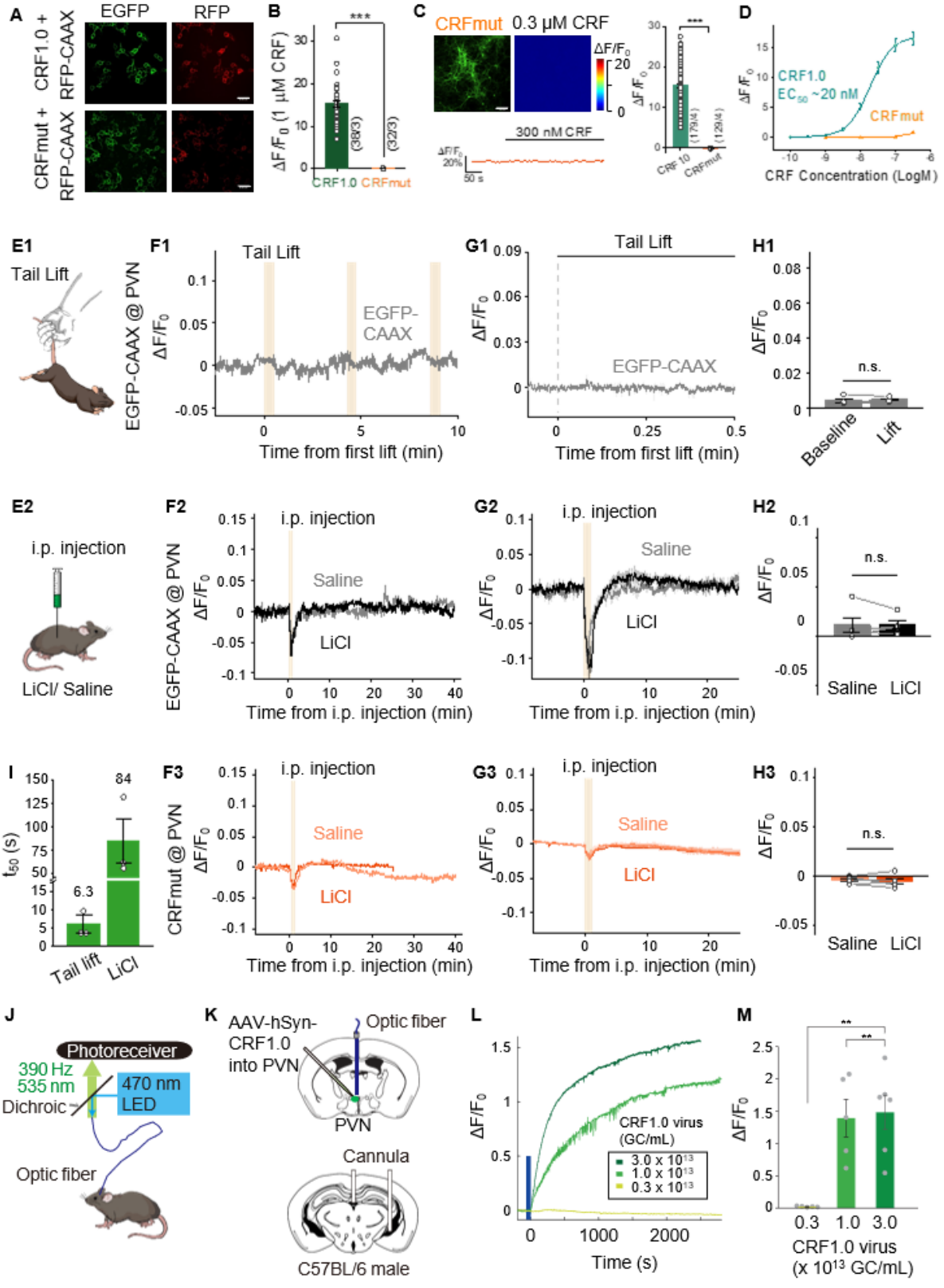

Fig. S13. CRF1.0 can detect endogenous CRF release using fiber photometry.

(**A**) Fluorescence images of HEK293T cells co-expressing RFP-CAAX together with CRF1.0 (top row) or CRFmut (bottom row). Scale bars, 100 μm.

(**B**) Summary of the change in fluorescence measured in cells expressing CRF1.0 or CRFmut in response to 1 μM CRF; n = 32-38 cells from 3 cultures.

(**C**) Expression and pseudocolor responses (upper left panel), a representative fluorescence trace (lower left panel), and summary of the response (right panel) measured in rat cortical neurons expressing CRFmut in response to 300 nM CRF; for comparison, the summary data also includes the response measured in neurons expressing CRF1.0 (n = 129-179 ROIs from 4-6 cultures). Scale bars, 100 μm.

(**D**) Dose-response curves measured in neurons expressing CRF1.0 or CRFmut in response to CRF; n = 3 cultures containing 20-40 neurons per culture.

(**E**) Schematic diagram depicting the experimental strategy. CRFmut or EGFP-CAAX was virally expressed in the paraventricular nucleus (PVN); 3 weeks later, the mice received a 30-s tail lift or an i.p. injection of LiCl or saline, and fluorescence was measured in the PVN.

(**F-H**) Representative fluorescence traces (**F**), average traces (**G**), and summary data (**H**) of CRFmut or EGFP-CAAX fluorescence in the PVN following a 30-s tail lift or an i.p. injection of saline or LiCl; n=5 and 4 animals for CRFmut and EGFP-CCAX group, respectively.

(**I**) Summary of the rise t_{50} values of the CRF1.0 signal in response to tail lift and i.p. injection of LiCl; n = 3 mice per group.

(**J**) Schematic illustration depicting the fiber photometry recording.

(**K**) Schematic diagrams depicting the virus injection site and optic fiber (top) and cannula implantation (bottom) locations.

(**L**) Representative traces showing CRF1.0 fluorescence (ΔF/F) before and after CRF infusion through the cannula. 1 mM CRF (4.8 mg/mL) was applied into one of the ventricles through implanted cannula with Hamilton syringe. CRH1.0-expressing AAV was injected 5 weeks before the recordings. The virus was undiluted (3.0×10^{13} GC/mL) or diluted using PBS to each a final titer of 1.0×10^{13} GC/mL (3-fold dilution) and 0.3×10^{13} GC/mL (10-fold dilution). Blue bar represents the timing of CRF application.

(**M**) Quantification of peak ΔF/F of CRF1.0 after CRF infusion through the cannula. **p<0.01 by one-way ANOVA test with Tukey's multiple comparisons test was performed. Error bars, S.E.M. n=5-6 animals.

Fig. S14. Expression of the peptide sensors has minimal effect on animal behaviors.

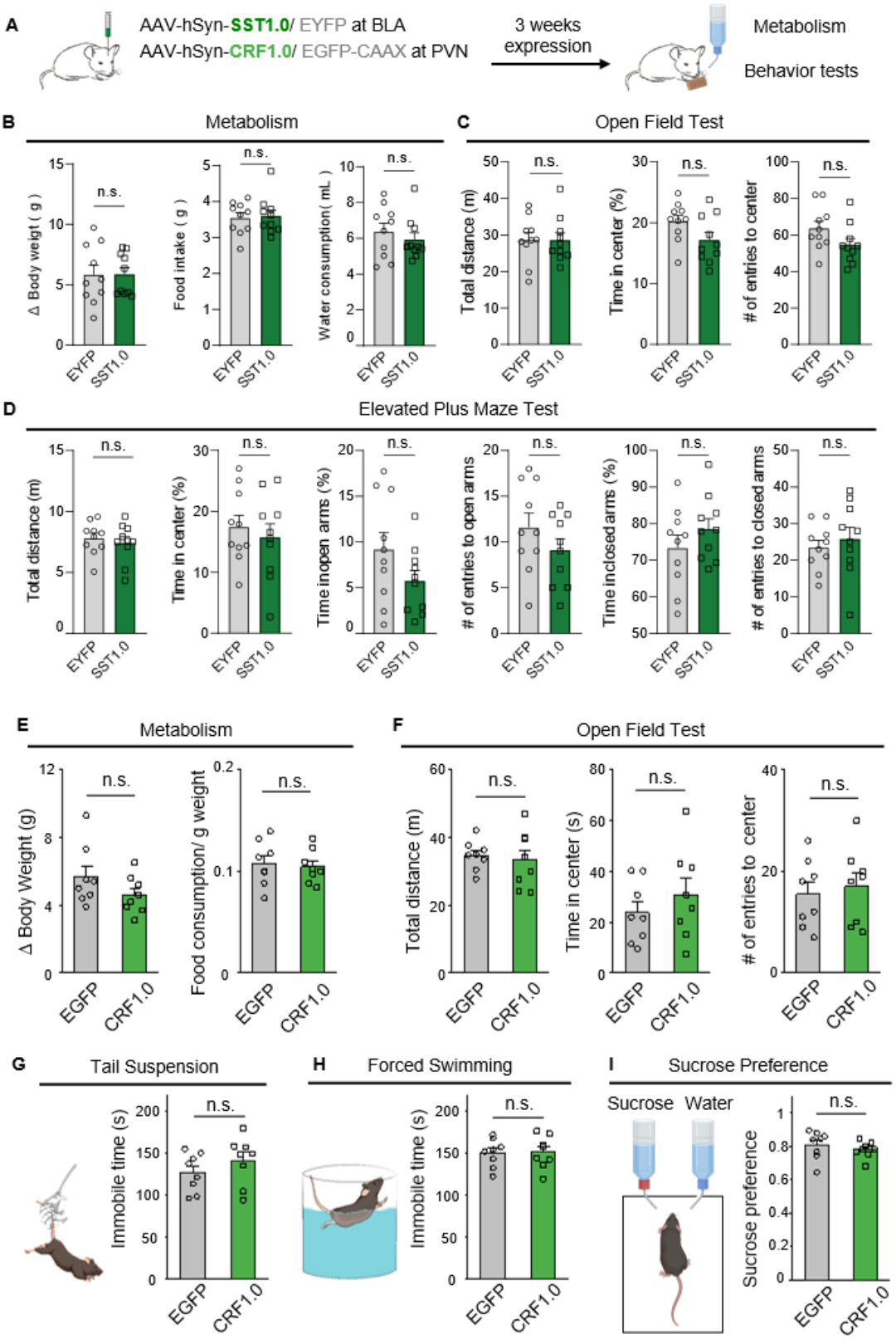

Fig. S14. Expression of the peptide sensors has minimal effect on animal behaviors.

(A) Schematic illustration depicting the experimental design in which GRAB peptide sensors or fluorescent protein controls was virally expressed; after 3 weeks expression, the metabolism and behaviors were tested.

(**B-D**) Quantification of metabolism parameters (**B**), behavioral parameters in the open field test (**C**), and behavioral parameters in the elevated plus maze test (**D**) of mice expressing SST1.0 or EYFP at BLA. n = 10 mice for each group, mean ± s.e.m., n.s., not significant.

(**E-I**) Quantification of metabolism parameters (**E**), behavioral parameters in the open field test (**F**), and behavioral parameters in the tail suspension test (**G**), forced swimming test (**H**) and sucrose preference test (**I**) of mice expressing CRF1.0 or EGFP-CAAX at PVN. n = 8 mice for each group, mean ± s.e.m., n.s., not significant.

Fig. S15. CRF1.0 can detect endogenous CRF release using 2-photon imaging.

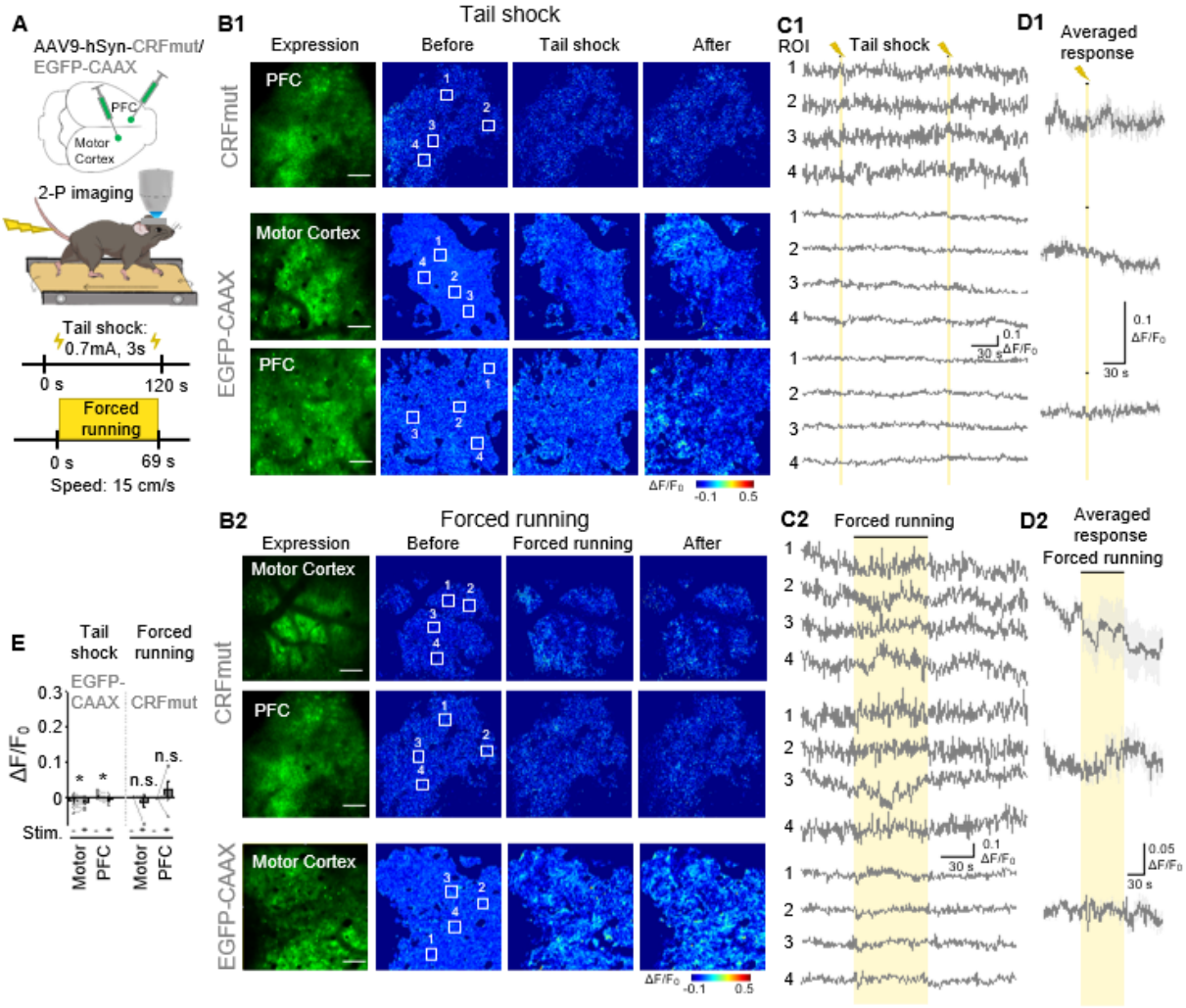

Fig. S15. CRF1.0 can detect endogenous CRF release using 2-photon imaging.

(**A-E**) Schematic diagram (**A**), representative fluorescence and pseudocolor images (**B**), representative traces of the indicated ROIs (**C**), average traces (**D**), and summary responses (**E**) measured in head-fixed mice expressing either CRFmut or EGFP-CAAX in the motor cortex and prefrontal cortex (PFC). Where indicated, the mice were subjected to the tail shock paradigm (**B1-D1**) or forced running on a treadmill (**B2-D2**) during two-photon *in vivo* imaging of the motor cortex and PFC. Scale bars, 100 μm.

Fig. S16. Validation of the CCK1.0 sensor in acute hippocampal slices.

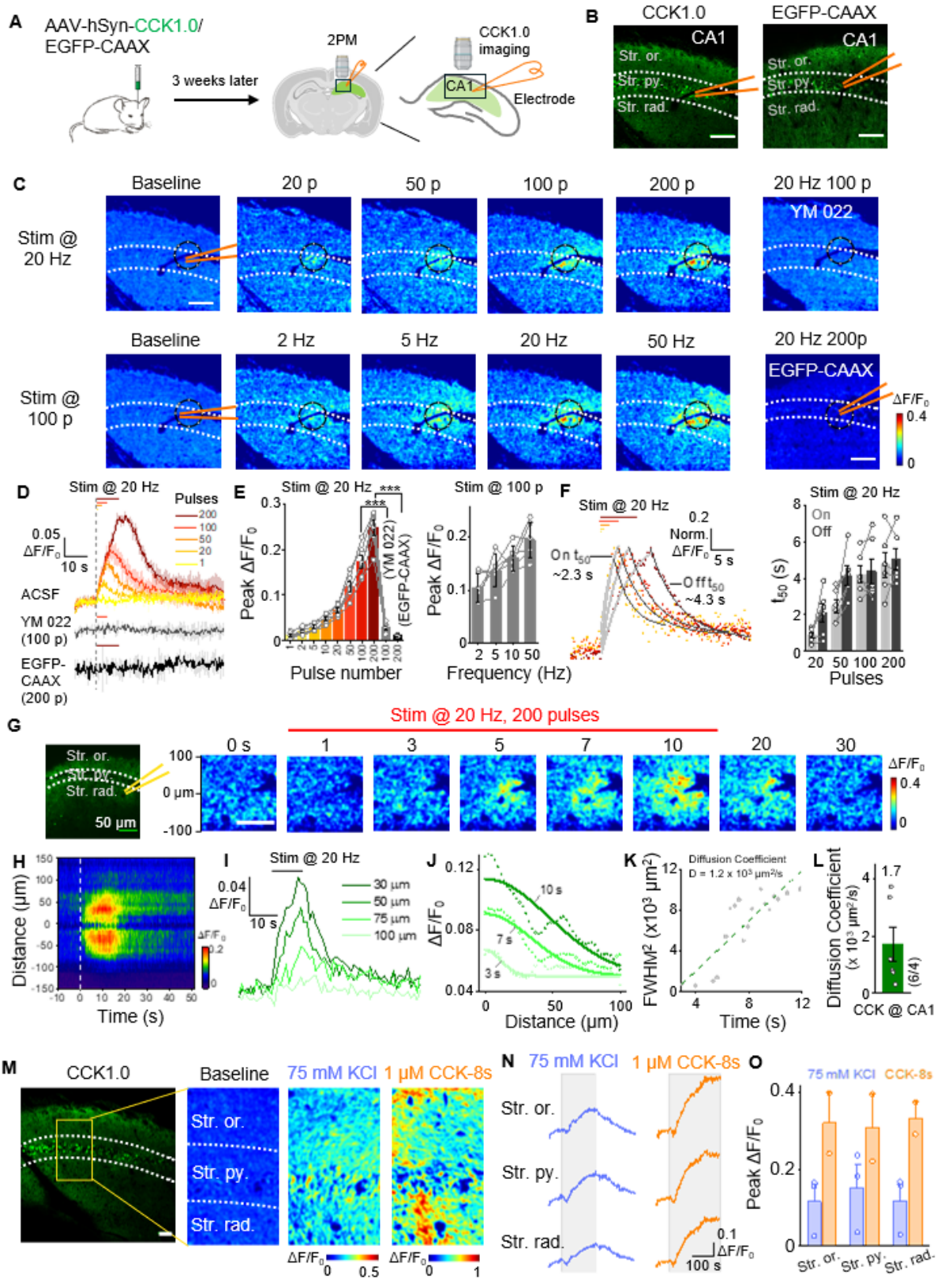

Fig. S16. Validation of the CCK1.0 sensor in acute hippocampal slices.

(**A**) Schematic illustration depicting the experimental design in which CCK1.0 or EGFP-CAAX was virally expressed in the mouse hippocampus; after 3 weeks, acute slices were prepared.

(**B**) Representative fluorescence images showing CCK1.0 or EGFP-CAAX expression in the CA1 region; the location of the stratum pyramidale, stratum oriens, and stratum radiatum are indicated, and the approximate location of the stimulating electrode is shown. Scale bars, 100 μm.

(**C**) Example pseudocolor images of CA1 slices expressing CCK1.measured at baseline and in response to 20, 50, 100, and 200 pulses delivered at 20 Hz (top row), or 100 pulses delivered at 2, 5, 20, and 50 Hz (bottom row). The images at the right show a slice treated with 10 μM YM 022 and stimulated with 100 pulses at 20 Hz (top) and a slice expressing EGFP-CAAX and stimulated with 200 pulses at 20 Hz (bottom). The black circles indicate the ROI used to analyze the responses.

(**D and E**) Representative traces (**D**) and summary (**E**) of the change in CCK1.0 fluorescence in response to various numbers of electric stimuli delivered in ACSF, 100 pulses delivered in YM 022, and the change in EGFP-CAAX fluorescence in response to 200 pulses. Shown at the right is the peak change in CCK1.0 fluorescence in response to 100 pulses delivered at the indicated frequencies. n = 2-6 slices from 1-4 mice.

(**F**) Representative fitted curves (left) and summary (right) of on and off t_{50} of the change in CCK1.0 fluorescence; n= 6 slices from 4 mice.

(**G**) Representative fluorescence image and example time-lapse pseudocolor images of CA1 slices expressing CCK1.0; during the first 10 s, 200 pulses were applied at 20 Hz. Scale bar, 50 μm (left), 100 μm (right).

(**H-J**) Representative spatial-temporal profile (**H**), temporal dynamics (**I**), and spatial dynamics (**J**) of the fluorescence change shown in (**G**). The profile in (**H**) shows the average response of three trials conducted in one slice. The traces in (**I**) and (**J**) correspond to the indicated distances and times, respectively, and the data in (**J**) were fitted with a Gaussian function.

(**K**) Representative plot of $FWHM^2$ (full width at half maximum, squared) against time using the data shown in (**J**); the diffusion coefficient (D) was measured as the slope of a line fitted to the data.

(**L**) Summary of the diffusion coefficient (D) for CCK measured in the CA1 region; n = 6 slices from 4 mice.

(**M-O**) Representative fluorescence and pseudocolor images (**M**), example traces (**N**), and summary peak response (**O**) of CCK1.0-expressing hippocampal slices in response to 75 mM KCl or 1 μM CCK-8s; n= 2-3 slices per group. Scale bar, 50 μm.

Fig. S17. Application of CRF induced similar CRF1.0 response among different cell types in brain slices.

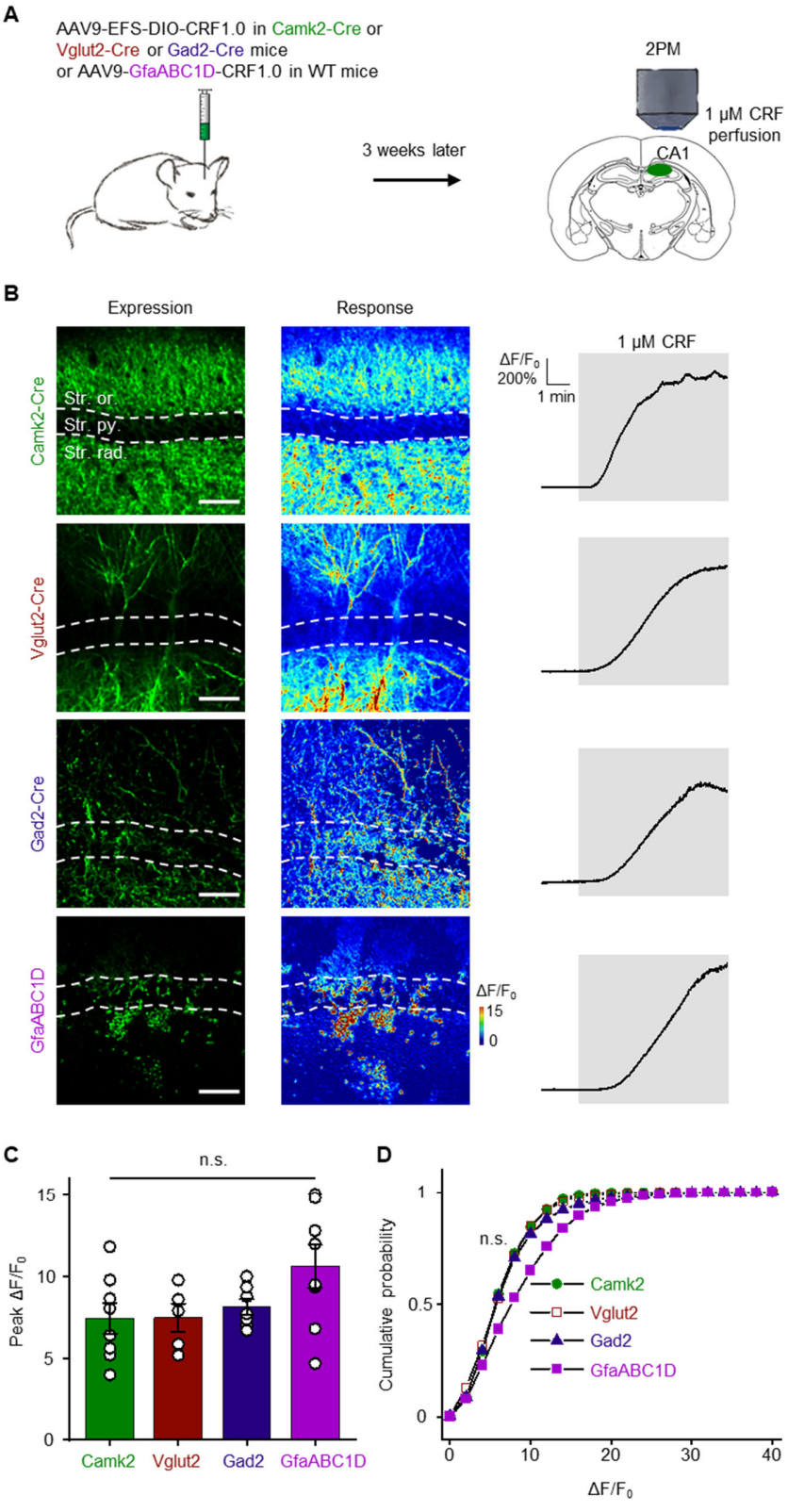

Fig. S17. Application of CRF induced similar CRF1.0 response among different cell types in brain slices.

(**A**) Schematic diagram of multiple cell types expressing CRF1.0 at CA1 in acute brain slices, treated with 1 μM CRF perfusion.

(**B**) Representative images showing the expression of the CRF1.0 sensor at CA1 (top), and pseudocolor images (middle) and example traces (bottom) showing the fluorescence change of CRF1.0 in response to 1 μM CRF perfusion. The expression images are calculated from CRF treated images subtracting basal images. Top 5% pixels in fluorescence intensity of the expression images are used to calculate the $\Delta F/F_0$ of traces. Scale bars, 100 μm.

(**C**) Summary of the peak responses of CRF1.0 signal in (B). Camk2: n=8 slices of 2 mice, Vglut2: n=8 slices of 2 mice; Gad2: n=7 slices of 3 mice; GfaABC1D: n=8 slices of 2 mice; One-way ANOVA, p=0.09.

(**D**) Cumulative probability plot of CRF1.0 $\Delta F/F_0$ measured in (B). Top 5% pixels are used to calculate the distribution. Kruskal-Wallis ANOVA, p=0.20.

Summary data are presented as the mean ± SEM. n.s., not significant.

Sensors	TM5 and N-terminal linker	cpGFP	C-terminal linker and TM6
GRAB-NE	P$^{5.72}$PSRRGPDAVAAPPGGTERRPNGLGPERSAGPGGAEAEPLPTQLNGAPGEPAPAGPRDTDALDLEEGG	cpGFP	TGAAARWRGRQN$^{6.28}$
GRAB-DA	V$^{5.72}$NTKRSSRAFRAHLRAPLKGNCTHPEDMKLGG	cpGFP	TGAAAMSRRKLSQQ$^{6.28}$
GRAB-ACh	GG	cpGFP	HNAK
GRAB-5-HT	M$^{5.71}$FLNG	cpGFP	GFATAN$^{6.28}$
dLight	LSSLI	cpGFP	NHDQL

Table S1. Amino acid sequences of ICL3s from selected sensors

Amino acid sequences of the ICL3 domains in the GRAB-NE, GRAB-DA, GRAB-ACh, GRAB-5-HT, and dLight sensors.

Sensors	Responses (Maximum $\Delta F/F_0$)	Affinity (Apparent EC_{50}, nM)	Kinetics (s)	Ex/Em/ Isosbestic point (nm)
SST1.0	4.3±0.2	13±2 (SST-28) 69±12 (SST-14)	0.28±0.01 (on) 4.5±0.38 (off)	500/ 520/ 425
CRF1.0	12.0±0.4	33±5 (CRF) 69±6 (UCN1)	0.42±0.06 (on) 12±0.9 (off)	500/ 520/ 415
CCK1.0	8.4±0.3	4.1±1 (CCK-8s) 2.9±0.8 (CCK-4)	0.30±0.05 (on) 18±1.4 (off)	505/ 520/ 425
NPY1.0	4.9±0.1	43±7 (NPY)	0.37±0.04 (on)	500/ 520/ 425
VIP1.0	3.6±0.2	19±5 (VIP)	0.91±0.08 (on)	500/ 520/ 420
NTS1.0	2.5±0.1	6.2±0.8 (NTS)	0.20±0.02 (on) 14±0.9 (off)	500/ 520/ 425

Table S2. Characterization of neuropeptide sensors expressed on HEK293T cells.

Sensors	Responses (Maximum $\Delta F/F_0$)	Sensor affinity (Apparent EC_{50}, nM)	Native receptor affinity (nM)	References
SST1.0	4.5±0.2	35±3 (SST-28) 130±12 (SST-14)	0.07-6.1 (SST-28) 0.53-4.1 (SST-14)	(*82-84*)
CRF1.0	12.6±0.8	18.6±1.6 (CRF)	5.2-229 (CRF)	(*85-88*)
CCK1.0	7.8±0.2	5.5±0.5 (CCK-8s)	0.12-0.27 (CCK-8s)	(*89-91*)
NPY1.0	4.2±0.1	0.7±0.03 (NPY)	0.7-2.1 (NPY)	(*92, 93*)
VIP1.0	3.2±0.1	19±3 (VIP)	1.7-16 (VIP)	(*94, 95*)
NTS1.0	3.0±0.1	7.8±0.8 (NTS)	0.2-5 (NTS)	(*96, 97*)

Table S3. Characterization of neuropeptide sensors expressed on cultured neurons and comparison of sensors' affinity with native receptors.

Uncorrected Fisher's LSD	Predicted (LS) mean diff.	95.00% CI of diff.	Summary	Individual P Value
1 vs. 3	-0.07704	-0.1564 to 0.002314	ns	0.0563
1 vs. 5	-0.1399	-0.2116 to -0.06826	***	0.0008
1 vs. 10	-0.2098	-0.2842 to -0.1353	****	<0.0001
1 vs. 16	-0.1845	-0.2619 to -0.1071	***	0.0001
3 vs. 5	-0.06289	-0.1377 to 0.01187	ns	0.0935
3 vs. 10	-0.1327	-0.2100 to -0.05540	**	0.0022
3 vs. 16	-0.1075	-0.1820 to -0.03301	**	0.0075
5 vs. 10	-0.06981	-0.1399 to 0.0002425	ns	0.0507
5 vs. 16	-0.04459	-0.1172 to 0.02802	ns	0.2114
10 vs. 16	0.02522	-0.04486 to 0.09530	ns	0.4566

Table S4. Multiple comparisons of responses elicited by pulse trains from Fig. 3C.

Movie S1.
Glucose stimulated SST release in isolated pancreatic islets, related to **Fig. 3**.

Data S1.
RNA-seq data of mice cortex tissue expressing peptide sensors or EGFP-CAAX, related to **Fig. 2H**.

Data S2.
RNA-seq data of rat cortical neurons and mice cortex tissue expressing peptide sensors or control fluorescent proteins, related to **Fig. S7**.

References and Notes

1. D. De Wied, E. R. De Kloet, Pro-opiomelanocortin (POMC) as homeostatic control system. *Ann. N. Y. Acad. Sci.* **512**, 328–337 (1987). doi:10.1111/j.1749-6632.1987.tb24971.x Medline

2. J. Spiess, J. Rivier, C. Rivier, W. Vale, Primary structure of corticotropin-releasing factor from ovine hypothalamus. *Proc. Natl. Acad. Sci. U.S.A.* **78**, 6517–6521 (1981). doi:10.1073/pnas.78.10.6517 Medline

3. A. V. Schally, A. Arimura, A. J. Kastin, Hypothalamic regulatory hormones. *Science* **179**, 341–350 (1973). doi:10.1126/science.179.4071.341 Medline

4. V. Du Vigneaud, Hormones of the posterior pituitary gland: Oxytocin and vasopressin. *Harvey Lect.* **50**, 1–26 (1954-1955). Medline

5. A. L. Alhadeff, Z. Su, E. Hernandez, M. L. Klima, S. Z. Phillips, R. A. Holland, C. Guo, A. W. Hantman, B. C. De Jonghe, J. N. Betley, A neural circuit for the suppression of pain by a competing need state. *Cell* **173**, 140–152.e15 (2018). doi:10.1016/j.cell.2018.02.057 Medline

6. L. de Lecea, T. S. Kilduff, C. Peyron, X. Gao, P. E. Foye, P. E. Danielson, C. Fukuhara, E. L. F. Battenberg, V. T. Gautvik, F. S. Bartlett 2nd, W. N. Frankel, A. N. van den Pol, F. E. Bloom, K. M. Gautvik, J. G. Sutcliffe, The hypocretins: Hypothalamus-specific peptides with neuroexcitatory activity. *Proc. Natl. Acad. Sci. U.S.A.* **95**, 322–327 (1998). doi:10.1073/pnas.95.1.322 Medline

7. T. Sakurai, A. Amemiya, M. Ishii, I. Matsuzaki, R. M. Chemelli, H. Tanaka, S. C. Williams, J. A. Richardson, G. P. Kozlowski, S. Wilson, J. R. S. Arch, R. E. Buckingham, A. C. Haynes, S. A. Carr, R. S. Annan, D. E. McNulty, W.-S. Liu, J. A. Terrett, N. A. Elshourbagy, D. J. Bergsma, M. Yanagisawa, Orexins and orexin receptors: A family of hypothalamic neuropeptides and G protein-coupled receptors that regulate feeding behavior. *Cell* **92**, 573–585 (1998). doi:10.1016/S0092-8674(00)80949-6 Medline

8. W. Vale, J. Spiess, C. Rivier, J. Rivier, Characterization of a 41-residue ovine hypothalamic peptide that stimulates secretion of corticotropin and β-endorphin. *Science* **213**, 1394–1397 (1981). doi:10.1126/science.6267699 Medline

9. A. S. Hauser, M. M. Attwood, M. Rask-Andersen, H. B. Schiöth, D. E. Gloriam, Trends in GPCR drug discovery: New agents, targets and indications. *Nat. Rev. Drug Discov.* **16**, 829–842 (2017). doi:10.1038/nrd.2017.178 Medline

10. A. P. Davenport, C. C. G. Scully, C. de Graaf, A. J. H. Brown, J. J. Maguire, Advances in therapeutic peptides targeting G protein-coupled receptors. *Nat. Rev. Drug Discov.* **19**, 389–413 (2020). doi:10.1038/s41573-020-0062-z Medline

11. T. Hökfelt, T. Bartfai, F. Bloom, Neuropeptides: Opportunities for drug discovery. *Lancet Neurol.* **2**, 463–472 (2003). doi:10.1016/S1474-4422(03)00482-4 Medline

12. J. S. Marvin, B. G. Borghuis, L. Tian, J. Cichon, M. T. Harnett, J. Akerboom, A. Gordus, S. L. Renninger, T.-W. Chen, C. I. Bargmann, M. B. Orger, E. R. Schreiter, J. B. Demb, W.-B. Gan, S. A. Hires, L. L. Looger, An optimized fluorescent probe for visualizing

glutamate neurotransmission. *Nat. Methods* **10**, 162–170 (2013). doi:10.1038/nmeth.2333 Medline

13. E. K. Unger, J. P. Keller, M. Altermatt, R. Liang, A. Matsui, C. Dong, O. J. Hon, Z. Yao, J. Sun, S. Banala, M. E. Flanigan, D. A. Jaffe, S. Hartanto, J. Carlen, G. O. Mizuno, P. M. Borden, A. V. Shivange, L. P. Cameron, S. Sinning, S. M. Underhill, D. E. Olson, S. G. Amara, D. Temple Lang, G. Rudnick, J. S. Marvin, L. D. Lavis, H. A. Lester, V. A. Alvarez, A. J. Fisher, J. A. Prescher, T. L. Kash, V. Yarov-Yarovoy, V. Gradinaru, L. L. Looger, L. Tian, Directed evolution of a selective and sensitive serotonin sensor via machine learning. *Cell* **183**, 1986–2002.e26 (2020). doi:10.1016/j.cell.2020.11.040 Medline

14. P. M. Borden, P. Zhang, A. V. Shivange, J. S. Marvin, J. Cichon, C. Dan, K. Podgorski, A. Figueiredo, O. Novak, M. Tanimoto, E. Shigetomi, M. A. Lobas, H. Kim, P. K. Zhu, Y. Zhang, W. S. Zheng, C. Fan, G. Wang, B. Xiang, L. Gan, G.-X. Zhang, K. Guo, L. Lin, Y. Cai, A. G. Yee, A. Aggarwal, C. P. Ford, D. C. Rees, D. Dietrich, B. S. Khakh, J. S. Dittman, W.-B. Gan, M. Koyama, V. Jayaraman, J. F. Cheer, H. A. Lester, J. J. Zhu, L. L. Looger, A fast genetically encoded fluorescent sensor for faithful in vivo acetylcholine detection in mice, fish, worms and flies. bioRxiv 2020.02.07.939504 [Preprint] (2020); https://doi.org/10.1101/2020.02.07.939504.

15. S. R. Foster, A. S. Hauser, L. Vedel, R. T. Strachan, X.-P. Huang, A. C. Gavin, S. D. Shah, A. P. Nayak, L. M. Haugaard-Kedström, R. B. Penn, B. L. Roth, H. Bräuner-Osborne, D. E. Gloriam, Discovery of human signaling systems: pairing peptides to G protein-coupled receptors. *Cell* **179**, 895–908.e21 (2019). doi:10.1016/j.cell.2019.10.010 Medline

16. V. Isberg, S. Mordalski, C. Munk, K. Rataj, K. Harpsøe, A. S. Hauser, B. Vroling, A. J. Bojarski, G. Vriend, D. E. Gloriam, GPCRdb: An information system for G protein-coupled receptors. *Nucleic Acids Res.* **44**, D356–D364 (2016). doi:10.1093/nar/gkv1178 Medline

17. M. Jing, P. Zhang, G. Wang, J. Feng, L. Mesik, J. Zeng, H. Jiang, S. Wang, J. C. Looby, N. A. Guagliardo, L. W. Langma, J. Lu, Y. Zuo, D. A. Talmage, L. W. Role, P. Q. Barrett, L. I. Zhang, M. Luo, Y. Song, J. J. Zhu, Y. Li, A genetically encoded fluorescent acetylcholine indicator for *in vitro* and *in vivo* studies. *Nat. Biotechnol.* **36**, 726–737 (2018). doi:10.1038/nbt.4184 Medline

18. F. Sun, J. Zeng, M. Jing, J. Zhou, J. Feng, S. F. Owen, Y. Luo, F. Li, H. Wang, T. Yamaguchi, Z. Yong, Y. Gao, W. Peng, L. Wang, S. Zhang, J. Du, D. Lin, M. Xu, A. C. Kreitzer, G. Cui, Y. Li, A genetically encoded fluorescent sensor enables rapid and specific detection of dopamine in flies, fish, and mice. *Cell* **174**, 481–496.e19 (2018). doi:10.1016/j.cell.2018.06.042 Medline

19. J. Feng, C. Zhang, J. E. Lischinsky, M. Jing, J. Zhou, H. Wang, Y. Zhang, A. Dong, Z. Wu, H. Wu, W. Chen, P. Zhang, J. Zou, S. A. Hires, J. J. Zhu, G. Cui, D. Lin, J. Du, Y. Li, A genetically encoded fluorescent sensor for rapid and specific in vivo detection of norepinephrine. *Neuron* **102**, 745–761.e8 (2019). doi:10.1016/j.neuron.2019.02.037 Medline

20. M. Jing, Y. Li, J. Zeng, P. Huang, M. Skirzewski, O. Kljakic, W. Peng, T. Qian, K. Tan, J. Zou, S. Trinh, R. Wu, S. Zhang, S. Pan, S. A. Hires, M. Xu, H. Li, L. M. Saksida, V. F.

Prado, T. J. Bussey, M. A. M. Prado, L. Chen, H. Cheng, Y. Li, An optimized acetylcholine sensor for monitoring *in vivo* cholinergic activity. *Nat. Methods* **17**, 1139–1146 (2020). doi:10.1038/s41592-020-0953-2 Medline

21. T. Patriarchi, J. R. Cho, K. Merten, M. W. Howe, A. Marley, W.-H. Xiong, R. W. Folk, G. J. Broussard, R. Liang, M. J. Jang, H. Zhong, D. Dombeck, M. von Zastrow, A. Nimmerjahn, V. Gradinaru, J. T. Williams, L. Tian, Ultrafast neuronal imaging of dopamine dynamics with designed genetically encoded sensors. *Science* **360**, eaat4422 (2018). doi:10.1126/science.aat4422 Medline

22. T. Qian, H. Wang, P. Wang, L. Geng, L. Mei, T. Osakada, L. Wang, Y. Tang, A. Kania, V. Grinevich, R. Stoop, D. Lin, M. Luo, Y. Li, A genetically encoded sensor measures temporal oxytocin release from different neuronal compartments. *Nat. Biotechnol.* **41**, 944–957 (2023). doi:10.1038/s41587-022-01561-2 Medline

23. D. Ino, Y. Tanaka, H. Hibino, M. Nishiyama, A fluorescent sensor for real-time measurement of extracellular oxytocin dynamics in the brain. *Nat. Methods* **19**, 1286–1294 (2022). doi:10.1038/s41592-022-01597-x Medline

24. L. Duffet, S. Kosar, M. Panniello, B. Viberti, E. Bracey, A. D. Zych, A. Radoux-Mergault, X. Zhou, J. Dernic, L. Ravotto, Y.-C. Tsai, M. Figueiredo, S. K. Tyagarajan, B. Weber, M. Stoeber, N. Gogolla, M. H. Schmidt, A. R. Adamantidis, T. Fellin, D. Burdakov, T. Patriarchi, A genetically encoded sensor for in vivo imaging of orexin neuropeptides. *Nat. Methods* **19**, 231–241 (2022). doi:10.1038/s41592-021-01390-2 Medline

25. J. M. Otaki, S. Firestein, Length analyses of mammalian G-protein-coupled receptors. *J. Theor. Biol.* **211**, 77–100 (2001). doi:10.1006/jtbi.2001.2272 Medline

26. H. Unal, S. S. Karnik, Domain coupling in GPCRs: The engine for induced conformational changes. *Trends Pharmacol. Sci.* **33**, 79–88 (2012). doi:10.1016/j.tips.2011.09.007 Medline

27. K. Hollenstein, J. Kean, A. Bortolato, R. K. Y. Cheng, A. S. Doré, A. Jazayeri, R. M. Cooke, M. Weir, F. H. Marshall, Structure of class B GPCR corticotropin-releasing factor receptor 1. *Nature* **499**, 438–443 (2013). doi:10.1038/nature12357 Medline

28. S. Ma, Q. Shen, L.-H. Zhao, C. Mao, X. E. Zhou, D.-D. Shen, P. W. de Waal, P. Bi, C. Li, Y. Jiang, M.-W. Wang, P. M. Sexton, D. Wootten, K. Melcher, Y. Zhang, H. E. Xu, Molecular basis for hormone recognition and activation of corticotropin-releasing factor receptors. *Mol. Cell* **77**, 669–680.e4 (2020). doi:10.1016/j.molcel.2020.01.013 Medline

29. W. Zhao, S. Han, N. Qiu, W. Feng, M. Lu, W. Zhang, M. Wang, Q. Zhou, S. Chen, W. Xu, J. Du, X. Chu, C. Yi, A. Dai, L. Hu, M. Y. Shen, Y. Sun, Q. Zhang, Y. Ma, W. Zhong, D. Yang, M.-W. Wang, B. Wu, Q. Zhao, Structural insights into ligand recognition and selectivity of somatostatin receptors. *Cell Res.* **32**, 761–772 (2022). doi:10.1038/s41422-022-00679-x Medline

30. A. Paul, M. Crow, R. Raudales, M. He, J. Gillis, Z. J. Huang, Transcriptional architecture of synaptic communication delineates GABAergic neuron identity. *Cell* **171**, 522–539.e20 (2017). doi:10.1016/j.cell.2017.08.032 Medline

31. S. J. Smith, U. Sümbül, L. T. Graybuck, F. Collman, S. Seshamani, R. Gala, O. Gliko, L. Elabbady, J. A. Miller, T. E. Bakken, J. Rossier, Z. Yao, E. Lein, H. Zeng, B. Tasic, M.

Hawrylycz, Single-cell transcriptomic evidence for dense intracortical neuropeptide networks. *eLife* **8**, e47889 (2019). doi:10.7554/eLife.47889 Medline

32. W. Zhong, S. Barde, N. Mitsios, C. Adori, P. Oksvold, K. V. Feilitzen, L. O'Leary, L. Csiba, T. Hortobágyi, P. Szocsics, N. Mechawar, Z. Maglóczky, É. Renner, M. Palkovits, M. Uhlén, J. Mulder, T. Hökfelt, The neuropeptide landscape of human prefrontal cortex. *Proc. Natl. Acad. Sci. U.S.A.* **119**, e2123146119 (2022). doi:10.1073/pnas.2123146119 Medline

33. F. Sun, J. Zhou, B. Dai, T. Qian, J. Zeng, X. Li, Y. Zhuo, Y. Zhang, Y. Wang, C. Qian, K. Tan, J. Feng, H. Dong, D. Lin, G. Cui, Y. Li, Next-generation GRAB sensors for monitoring dopaminergic activity in vivo. *Nat. Methods* **17**, 1156–1166 (2020). doi:10.1038/s41592-020-00981-9 Medline

34. J. Wan, W. Peng, X. Li, T. Qian, K. Song, J. Zeng, F. Deng, S. Hao, J. Feng, P. Zhang, Y. Zhang, J. Zou, S. Pan, M. Shin, B. J. Venton, J. J. Zhu, M. Jing, M. Xu, Y. Li, A genetically encoded sensor for measuring serotonin dynamics. *Nat. Neurosci.* **24**, 746–752 (2021). doi:10.1038/s41593-021-00823-7 Medline

35. F. M. Dautzenberg, E. Gutknecht, I. Van der Linden, J. A. Olivares-Reyes, F. Dürrenberger, R. L. Hauger, Cell-type specific calcium signaling by corticotropin-releasing factor type 1 (CRF_1) and 2a ($CRF_{2(a)}$) receptors: phospholipase C-mediated responses in human embryonic kidney 293 but not SK-N-MC neuroblastoma cells. *Biochem. Pharmacol.* **68**, 1833–1844 (2004). doi:10.1016/j.bcp.2004.07.013 Medline

36. B. Wamsley, G. Fishell, Genetic and activity-dependent mechanisms underlying interneuron diversity. *Nat. Rev. Neurosci.* **18**, 299–309 (2017). doi:10.1038/nrn.2017.30 Medline

37. C. M. Persoon, A. Moro, J. P. Nassal, M. Farina, J. H. Broeke, S. Arora, N. Dominguez, J. R. T. van Weering, R. F. Toonen, M. Verhage, Pool size estimations for dense-core vesicles in mammalian CNS neurons. *EMBO J.* **37**, e99672 (2018). doi:10.15252/embj.201899672 Medline

38. S. Arora, I. Saarloos, R. Kooistra, R. van de Bospoort, M. Verhage, R. F. Toonen, SNAP-25 gene family members differentially support secretory vesicle fusion. *J. Cell Sci.* **130**, 1877–1889 (2017). doi:10.1242/jcs.201889 Medline

39. U. Kumar, S. Singh, Role of somatostatin in the regulation of central and peripheral factors of satiety and obesity. *Int. J. Mol. Sci.* **21**, 2568 (2020). doi:10.3390/ijms21072568 Medline

40. A. C. Hauge-Evans, A. J. King, D. Carmignac, C. C. Richardson, I. C. A. F. Robinson, M. J. Low, M. R. Christie, S. J. Persaud, P. M. Jones, Somatostatin secreted by islet δ-cells fulfills multiple roles as a paracrine regulator of islet function. *Diabetes* **58**, 403–411 (2009). doi:10.2337/db08-0792 Medline

41. P. Rorsman, M. O. Huising, The somatostatin-secreting pancreatic δ-cell in health and disease. *Nat. Rev. Endocrinol.* **14**, 404–414 (2018). doi:10.1038/s41574-018-0020-6 Medline

42. A. Salehi, S. S. Qader, E. Grapengiesser, B. Hellman, Pulses of somatostatin release are slightly delayed compared with insulin and antisynchronous to glucagon. *Regul. Pept.* **144**, 43–49 (2007). doi:10.1016/j.regpep.2007.06.003 Medline

43. B. Hellman, A. Salehi, E. Grapengiesser, E. Gylfe, Isolated mouse islets respond to glucose with an initial peak of glucagon release followed by pulses of insulin and somatostatin in antisynchrony with glucagon. *Biochem. Biophys. Res. Commun.* **417**, 1219–1223 (2012). doi:10.1016/j.bbrc.2011.12.113 Medline

44. T. Reisine, G. I. Bell, Molecular biology of somatostatin receptors. *Endocr. Rev.* **16**, 427–442 (1995). Medline

45. O. Nakagawasai, S. Hozumi, K. Tan-No, F. Niijima, Y. Arai, H. Yasuhara, T. Tadano, Immunohistochemical fluorescence intensity reduction of brain somatostatin in the impairment of learning and memory-related behaviour induced by olfactory bulbectomy. *Behav. Brain Res.* **142**, 63–67 (2003). doi:10.1016/S0166-4328(02)00383-2 Medline

46. P. Davies, R. Katzman, R. D. Terry, Reduced somatostatin-like immunoreactivity in cerebral cortex from cases of Alzheimer disease and Alzheimer senile dementia. *Nature* **288**, 279–280 (1980). doi:10.1038/288279a0 Medline

47. C. Kluge, C. Stoppel, C. Szinyei, O. Stork, H. C. Pape, Role of the somatostatin system in contextual fear memory and hippocampal synaptic plasticity. *Learn. Mem.* **15**, 252–260 (2008). doi:10.1101/lm.793008 Medline

48. J. M. Stujenske, P.-K. O'Neill, C. Fernandes-Henriques, I. Nahmoud, S. R. Goldburg, A. Singh, L. Diaz, M. Labkovich, W. Hardin, S. S. Bolkan, T. R. Reardon, T. J. Spellman, C. D. Salzman, J. A. Gordon, C. Liston, E. Likhtik, Prelimbic cortex drives discrimination of non-aversion via amygdala somatostatin interneurons. *Neuron* **110**, 2258–2267.e11 (2022). doi:10.1016/j.neuron.2022.03.020 Medline

49. J. Gründemann, A. Lüthi, Ensemble coding in amygdala circuits for associative learning. *Curr. Opin. Neurobiol.* **35**, 200–206 (2015). doi:10.1016/j.conb.2015.10.005 Medline

50. P. H. Janak, K. M. Tye, From circuits to behaviour in the amygdala. *Nature* **517**, 284–292 (2015). doi:10.1038/nature14188 Medline

51. Y. S. Jo, V. M. K. Namboodiri, G. D. Stuber, L. S. Zweifel, Persistent activation of central amygdala CRF neurons helps drive the immediate fear extinction deficit. *Nat. Commun.* **11**, 422 (2020). doi:10.1038/s41467-020-14393-y Medline

52. C. A. Sanford, M. E. Soden, M. A. Baird, S. M. Miller, J. Schulkin, R. D. Palmiter, M. Clark, L. S. Zweifel, A central amygdala CRF circuit facilitates learning about weak threats. *Neuron* **93**, 164–178 (2017). doi:10.1016/j.neuron.2016.11.034 Medline

53. M. B. Pomrenze, J. Tovar-Diaz, A. Blasio, R. Maiya, S. M. Giovanetti, K. Lei, H. Morikawa, F. W. Hopf, R. O. Messing, A corticotropin releasing factor network in the extended amygdala for anxiety. *J. Neurosci.* **39**, 1030–1043 (2019). doi:10.1523/JNEUROSCI.2143-18.2018 Medline

54. G. de Guglielmo, M. Kallupi, M. B. Pomrenze, E. Crawford, S. Simpson, P. Schweitzer, G. F. Koob, R. O. Messing, O. George, Inactivation of a CRF-dependent amygdalofugal pathway reverses addiction-like behaviors in alcohol-dependent rats. *Nat. Commun.* **10**, 1238 (2019). doi:10.1038/s41467-019-09183-0 Medline

55. J. Kim, S. Lee, Y.-Y. Fang, A. Shin, S. Park, K. Hashikawa, S. Bhat, D. Kim, J.-W. Sohn, D. Lin, G. S. B. Suh, Rapid, biphasic CRF neuronal responses encode positive and negative valence. *Nat. Neurosci.* **22**, 576–585 (2019). doi:10.1038/s41593-019-0342-2 Medline

56. Y. Yuan, W. Wu, M. Chen, F. Cai, C. Fan, W. Shen, W. Sun, J. Hu, Reward inhibits paraventricular CRH neurons to relieve stress. *Curr. Biol.* **29**, 1243–1251.e4 (2019). doi:10.1016/j.cub.2019.02.048 Medline

57. N. Daviu, T. Füzesi, D. G. Rosenegger, N. P. Rasiah, T.-L. Sterley, G. Peringod, J. S. Bains, Paraventricular nucleus CRH neurons encode stress controllability and regulate defensive behavior selection. *Nat. Neurosci.* **23**, 398–410 (2020). doi:10.1038/s41593-020-0591-0 Medline

58. T. Gallopin, H. Geoffroy, J. Rossier, B. Lambolez, Cortical sources of CRF, NKB, and CCK and their effects on pyramidal cells in the neocortex. *Cereb. Cortex* **16**, 1440–1452 (2006). doi:10.1093/cercor/bhj081 Medline

59. J. M. Deussing, A. Chen, The corticotropin-releasing factor family: physiology of the stress response. *Physiol. Rev.* **98**, 2225–2286 (2018). doi:10.1152/physrev.00042.2017 Medline

60. P. Chen, S. Lou, Z.-H. Huang, Z. Wang, Q.-H. Shan, Y. Wang, Y. Yang, X. Li, H. Gong, Y. Jin, Z. Zhang, J.-N. Zhou, Prefrontal cortex corticotropin-releasing factor neurons control behavioral style selection under challenging situations. *Neuron* **106**, 301–315.e7 (2020). doi:10.1016/j.neuron.2020.01.033 Medline

61. A. Uribe-Mariño, N. C. Gassen, M. F. Wiesbeck, G. Balsevich, S. Santarelli, B. Solfrank, C. Dournes, G. R. Fries, M. Masana, C. Labermeier, X.-D. Wang, K. Hafner, B. Schmid, T. Rein, A. Chen, J. M. Deussing, M. V. Schmidt, Prefrontal cortex corticotropin-releasing factor receptor 1 conveys acute stress-induced executive dysfunction. *Biol. Psychiatry* **80**, 743–753 (2016). doi:10.1016/j.biopsych.2016.03.2106 Medline

62. T. A. Nielsen, D. A. DiGregorio, R. A. Silver, Modulation of glutamate mobility reveals the mechanism underlying slow-rising AMPAR EPSCs and the diffusion coefficient in the synaptic cleft. *Neuron* **42**, 757–771 (2004). doi:10.1016/j.neuron.2004.04.003 Medline

63. M. E. Rice, G. A. Gerhardt, P. M. Hierl, G. Nagy, R. N. Adams, Diffusion coefficients of neurotransmitters and their metabolites in brain extracellular fluid space. *Neuroscience* **15**, 891–902 (1985). doi:10.1016/0306-4522(85)90087-9 Medline

64. A. N. Weiss, M. A. Bittner, R. W. Holz, D. Axelrod, Protein mobility within secretory granules. *Biophys. J.* **107**, 16–25 (2014). doi:10.1016/j.bpj.2014.04.063 Medline

65. M. R. DiGruccio, A. M. Mawla, C. J. Donaldson, G. M. Noguchi, J. Vaughan, C. Cowing-Zitron, T. van der Meulen, M. O. Huising, Comprehensive alpha, beta and delta cell transcriptomes reveal that ghrelin selectively activates delta cells and promotes somatostatin release from pancreatic islets. *Mol. Metab.* **5**, 449–458 (2016). doi:10.1016/j.molmet.2016.04.007 Medline

66. M. O. Huising, T. van der Meulen, J. L. Huang, M. S. Pourhosseinzadeh, G. M. Noguchi, The difference δ-cells make in glucose control. *Physiology* **33**, 403–411 (2018). doi:10.1152/physiol.00029.2018 Medline

67. S. J. Smith, M. Hawrylycz, J. Rossier, U. Sümbül, New light on cortical neuropeptides and synaptic network plasticity. *Curr. Opin. Neurobiol.* **63**, 176–188 (2020). doi:10.1016/j.conb.2020.04.002 Medline

68. M. Ludwig, G. Leng, Dendritic peptide release and peptide-dependent behaviours. *Nat. Rev. Neurosci.* **7**, 126–136 (2006). doi:10.1038/nrn1845 Medline

69. A. N. van den Pol, Neuropeptide transmission in brain circuits. *Neuron* **76**, 98–115 (2012). doi:10.1016/j.neuron.2012.09.014 Medline

70. J. P. Overington, B. Al-Lazikani, A. L. Hopkins, How many drug targets are there? *Nat. Rev. Drug Discov.* **5**, 993–996 (2006). doi:10.1038/nrd2199 Medline

71. I. Nederpelt, J. Bunnik, A. P. IJzerman, L. H. Heitman, Kinetic profile of neuropeptide–receptor interactions. *Trends Neurosci.* **39**, 830–839 (2016). doi:10.1016/j.tins.2016.09.008 Medline

72. A. Kaiser, I. Coin, Capturing peptide-GPCR interactions and their dynamics. *Molecules* **25**, 4724 (2020). doi:10.3390/molecules25204724 Medline

73. E. B. De Souza, Corticotropin-releasing factor receptors in the rat central nervous system: Characterization and regional distribution. *J. Neurosci.* **7**, 88–100 (1987). doi:10.1523/JNEUROSCI.07-01-00088.1987 Medline

74. M. Castro, V. O. Nikolaev, D. Palm, M. J. Lohse, J. P. Vilardaga, Turn-on switch in parathyroid hormone receptor by a two-step parathyroid hormone binding mechanism. *Proc. Natl. Acad. Sci. U.S.A.* **102**, 16084–16089 (2005). doi:10.1073/pnas.0503942102 Medline

75. I. Nederpelt, V. Georgi, F. Schiele, K. Nowak-Reppel, A. E. Fernández-Montalván, A. P. IJzerman, L. H. Heitman, Characterization of 12 GnRH peptide agonists – a kinetic perspective. *Br. J. Pharmacol.* **173**, 128–141 (2016). doi:10.1111/bph.13342 Medline

76. W. Yin, Z. Li, M. Jin, Y.-L. Yin, P. W. de Waal, K. Pal, Y. Yin, X. Gao, Y. He, J. Gao, X. Wang, Y. Zhang, H. Zhou, K. Melcher, Y. Jiang, Y. Cong, X. Edward Zhou, X. Yu, H. Eric Xu, A complex structure of arrestin-2 bound to a G protein-coupled receptor. *Cell Res.* **29**, 971–983 (2019). doi:10.1038/s41422-019-0256-2 Medline

77. K. Yusa, L. Zhou, M. A. Li, A. Bradley, N. L. Craig, A hyperactive piggyBac transposase for mammalian applications. *Proc. Natl. Acad. Sci. U.S.A.* **108**, 1531–1536 (2011). doi:10.1073/pnas.1008322108 Medline

78. W. K. Kroeze, M. F. Sassano, X.-P. Huang, K. Lansu, J. D. McCorvy, P. M. Giguère, N. Sciaky, B. L. Roth, PRESTO-Tango as an open-source resource for interrogation of the druggable human GPCRome. *Nat. Struct. Mol. Biol.* **22**, 362–369 (2015). doi:10.1038/nsmb.3014 Medline

79. Q. Wan, N. Okashah, A. Inoue, R. Nehmé, B. Carpenter, C. G. Tate, N. A. Lambert, Mini G protein probes for active G protein–coupled receptors (GPCRs) in live cells. *J. Biol. Chem.* **293**, 7466–7473 (2018). doi:10.1074/jbc.RA118.001975 Medline

80. X. Y. Qin, Q.-H. Shan, H. Fang, Y. Wang, P. Chen, Z.-Q. Xiong, D. F. Swaab, J.-N. Zhou, PSD-93 up-regulates the synaptic activity of corticotropin-releasing hormone neurons in

the paraventricular nucleus in depression. *Acta Neuropathol.* **142**, 1045–1064 (2021). doi:10.1007/s00401-021-02371-7 Medline

81. Y. Zhu, G. Nachtrab, P. C. Keyes, W. E. Allen, L. Luo, X. Chen, Dynamic salience processing in paraventricular thalamus gates associative learning. *Science* **362**, 423–429 (2018). doi:10.1126/science.aat0481 Medline

82. Y. C. Patel, C. B. Srikant, Subtype selectivity of peptide analogs for all five cloned human somatostatin receptors (hsstr 1–5). *Endocrinology* **135**, 2814–2817 (1994). doi:10.1210/endo.135.6.7988476 Medline

83. C. Bruns, F. Raulf, D. Hoyer, J. Schloos, H. Lübbert, G. Weckbecker, Binding properties of somatostatin receptor subtypes. *Metabolism* **45** (suppl. 1), 17–20 (1996). doi:10.1016/S0026-0495(96)90072-4 Medline

84. S. Siehler, K. Seuwen, D. Hoyer, Characterisation of human recombinant somatostatin receptors. 1. Radioligand binding studies. *Naunyn Schmiedebergs Arch. Pharmacol.* **360**, 488–499 (1999). doi:10.1007/s002109900141 Medline

85. R. Chen, K. A. Lewis, M. H. Perrin, W. W. Vale, Expression cloning of a human corticotropin-releasing-factor receptor. *Proc. Natl. Acad. Sci. U.S.A.* **90**, 8967–8971 (1993). doi:10.1073/pnas.90.19.8967 Medline

86. F. M. Dautzenberg, K. Dietrich, M. R. Palchaudhuri, J. Spiess, Identification of two corticotropin-releasing factor receptors from *Xenopus laevis* with high ligand selectivity: Unusual pharmacology of the type 1 receptor. *J. Neurochem.* **69**, 1640–1649 (1997). doi:10.1046/j.1471-4159.1997.69041640.x Medline

87. J. Vaughan, C. Donaldson, J. Bittencourt, M. H. Perrin, K. Lewis, S. Sutton, R. Chan, A. V. Turnbull, D. Lovejoy, C. Rivier, J. Rivier, P. E. Sawchenko, W. Vale, Urocortin, a mammalian neuropeptide related to fish urotensin I and to corticotropin-releasing factor. *Nature* **378**, 287–292 (1995). doi:10.1038/378287a0 Medline

88. M. H. Perrin, W. W. Vale, Corticotropin releasing factor receptors and their ligand family. *Ann. N. Y. Acad. Sci.* **885**, 312–328 (1999). doi:10.1111/j.1749-6632.1999.tb08687.x Medline

89. M. Ito, T. Matsui, T. Taniguchi, T. Tsukamoto, T. Murayama, N. Arima, H. Nakata, T. Chiba, K. Chihara, Functional characterization of a human brain cholecystokinin-B receptor. A trophic effect of cholecystokinin and gastrin. *J. Biol. Chem.* **268**, 18300–18305 (1993). doi:10.1016/S0021-9258(17)46844-X Medline

90. Y. M. Lee, M. Beinborn, E. W. McBride, M. Lu, L. F. Kolakowski Jr., A. S. Kopin, The human brain cholecystokinin-B/gastrin receptor. Cloning and characterization. *J. Biol. Chem.* **268**, 8164–8169 (1993). doi:10.1016/S0021-9258(18)53076-3 Medline

91. J. Hughes, P. Boden, B. Costall, A. Domeney, E. Kelly, D. C. Horwell, J. C. Hunter, R. D. Pinnock, G. N. Woodruff, Development of a class of selective cholecystokinin type B receptor antagonists having potent anxiolytic activity. *Proc. Natl. Acad. Sci. U.S.A.* **87**, 6728–6732 (1990). doi:10.1073/pnas.87.17.6728 Medline

92. D. R. Gehlert, D. A. Schober, S. L. Gackenheimer, L. Beavers, R. Gadski, I. Lundell, D. Larhammar, [^{125}I]Leu^{31}, Pro^{34}-PYY is a high affinity radioligand for rat PP1/Y4 and Y1

receptors: Evidence for heterogeneity in pancreatic polypeptide receptors. *Peptides* **18**, 397–401 (1997). doi:10.1016/S0196-9781(96)00346-4 Medline

93. J. Krause, C. Eva, P. H. Seeburg, R. Sprengel, Neuropeptide Y1 subtype pharmacology of a recombinantly expressed neuropeptide receptor. *Mol. Pharmacol.* **41**, 817–821 (1992). Medline

94. M. Xia, S. P. Sreedharan, D. R. Bolin, G. O. Gaufo, E. J. Goetzl, Novel cyclic peptide agonist of high potency and selectivity for the type II vasoactive intestinal peptide receptor. *J. Pharmacol. Exp. Ther.* **281**, 629–633 (1997). Medline

95. P. Nicole, L. Lins, C. Rouyer-Fessard, C. Drouot, P. Fulcrand, A. Thomas, A. Couvineau, J. Martinez, R. Brasseur, M. Laburthe, Identification of key residues for interaction of vasoactive intestinal peptide with human $VPAC_1$ and $VPAC_2$ receptors and development of a highly selective $VPAC_1$ receptor agonist. Alanine scanning and molecular modeling of the peptide. *J. Biol. Chem.* **275**, 24003–24012 (2000). doi:10.1074/jbc.M002325200 Medline

96. B. Cusack, K. Jansen, D. J. McCormick, T. Chou, Y. Pang, E. Richelson, A single amino acid of the human and rat neurotensin receptors (subtype 1) determining the pharmacological profile of a species-selective neurotensin agonist. *Biochem. Pharmacol.* **60**, 793–801 (2000). doi:10.1016/S0006-2952(00)00409-3 Medline

97. F. Richard, S. Barroso, J. Martinez, C. Labbé-Jullié, P. Kitabgi, Agonism, inverse agonism, and neutral antagonism at the constitutively active human neurotensin receptor 2. *Mol. Pharmacol.* **60**, 1392–1398 (2001). doi:10.1124/mol.60.6.1392 Medline